

## **PlexinA4 mediates cytotoxic T cell trafficking and exclusion in cancer**

Ward Celus<sup>1,2,\*</sup>, Ana I. Oliveira<sup>1,2,3,4,\*</sup>, Silvia Ravis<sup>1,2</sup>, Heleen H. Van Acker<sup>1,2</sup>, Ewout Landeloos<sup>5,6</sup>, Jens Serneels<sup>1,2</sup>, Sarah Trusso Cafarello<sup>1,2</sup>, Yannick Van Herck<sup>7</sup>, Roberta Mastrantonio<sup>8</sup>, Arnaud Köhler<sup>9,10</sup>, Abhishek D. Garg<sup>11</sup>, Véronique Flamand<sup>9,10</sup>, Luca Tamagnone<sup>8,12</sup>, Jean-Christophe Marine<sup>5,6</sup>, Mario Di Matteo<sup>1,2</sup>, Bruno M. Costa<sup>3,4</sup>, Oliver Bechter<sup>7</sup>, Massimiliano Mazzone<sup>1,2,†</sup>

<sup>1</sup>Laboratory of Tumor Inflammation and Angiogenesis, Center for Cancer Biology, VIB, Leuven, Belgium.

<sup>2</sup>Laboratory of Tumor Inflammation and Angiogenesis, Department of Oncology, KU Leuven, Leuven, Belgium.

<sup>3</sup>Life and Health Sciences Research Institute (ICVS), School of Medicine, University of Minho, Braga, Portugal.

<sup>4</sup>ICVS/3B's - PT Government Associate Laboratory, Braga/Guimarães, University of Minho, Braga, Portugal.

<sup>5</sup>Laboratory for Molecular Cancer Biology, Center for Cancer Biology, VIB, Leuven, Belgium.

<sup>6</sup>Laboratory for Molecular Cancer Biology, Department of Oncology, KU Leuven, Leuven, Belgium.

<sup>7</sup>Department of General Medical Oncology, University Hospitals Leuven, Department of Oncology, KU Leuven, Leuven, Belgium.

<sup>8</sup>Department of Life Sciences and Public Health, Università Cattolica del Sacro Cuore, Rome, Italy.

<sup>9</sup>Institute for Medical Immunology, ULB-Center for Research in Immunology Gosselies, Belgium.

<sup>10</sup>Institute for Medical Immunology, Université Libre de Bruxelles, Gosselies, Belgium.

<sup>11</sup>Laboratory of Cell Stress & Immunity, Department of Cellular and Molecular Medicine, KU Leuven, Leuven, Belgium.

<sup>12</sup>Fondazione Policlinico "A. Gemelli"- IRCCS, Rome, Italy.

\*These authors contributed equally to this work.

†Corresponding author

### **Running title**

PlexinA4 mediates CTL trafficking and exclusion in cancer

### **Keywords**

Axon guidance molecules, PlexinA4, CTLs, T cell motility, Immunotherapy

### **Financial support**

This work was supported by the Research Foundation Flanders (FWO, G0A8219N). A.I.O. was supported by Fundação para a Ciência e Tecnologia (SFRH/BD/52287/2013) and by FWO under the project G0A8219N. W.C. was supported by an FWO-Strategic Basic Research (SB) doctoral fellowship (1S26917N). S.R. was supported by an FWO-Fundamental Research (FR) doctoral fellowship (1197720N). H.H.V.A. was supported by a fundamental postdoctoral mandate of the Belgian Foundation against Cancer (Stichting tegen Kanker). E.L. was funded

by Kom op tegen Kanker (Stand up to Cancer), the Flemish cancer society. A.K. and V.F. were funded by the FNRS (CDR 33685316 grant) and the Walloon Region (FEDER Wallonia-Biomed portfolio). A.D.G. was supported by FWO (G0B4620N; EOS grant: 30837538), KU Leuven (C14/19/098; POR/16/040) and Kom op Tegen Kanker (KOTK/2018/11509/1). E.L., O.B. and J.C.M. are funded within the Grand Challenge program of VIB, which received support from the Flemish Government under the Management Agreement 2017-2021 (VR 2016 2312 Doc.1521/4). B.M.C. was supported by the Northern Portugal Regional Operational Programme (NORTE 2020) under the project NORTE-01-0145-FEDER-000013 and the European Regional Development Fund (FEDER) under the Portugal 2020 Partnership Agreement. M.M. was granted by an ERC Consolidator Grant (773208) and by FWO (G0A8219N).

### **Corresponding author**

Massimiliano Mazzone

VIB Center for Cancer Biology, Department of Oncology, University of Leuven

Campus Gasthuisberg, Herestraat 49, box 912, B-3000 Leuven, Belgium

Tel: +32-16-37.32.13

Fax: +32-16-37.25.85

E-mail: [massimiliano.mazzone@kuleuven.be](mailto:massimiliano.mazzone@kuleuven.be)

### **Conflict of interest**

The authors have declared that no conflict of interest exists.

### **Manuscript details**

Word count: 5.774 words (excluding abstract, material and methods, references and figure legends)

Total number of figures/tables: 6 (excluding supplementary materials)

## **Abstract**

Cytotoxic T cell (CTL) infiltration of the tumor carries the potential to limit cancer progression, but their exclusion by the immunosuppressive tumor microenvironment hampers the efficiency of immunotherapy. Here, we show that expression of the axon guidance molecule PlexinA4 (*Plxna4*) in CTLs, especially in effector/memory CD8<sup>+</sup> T cells, is induced upon T-cell activation, sustained in the circulation, but reduced when entering the tumor bed. Therefore, we deleted *Plxna4* and observed that *Plxna4*-deficient CTLs acquired improved homing capacity to the lymph nodes and to the tumor, as well as increased proliferation, both achieved through enhanced Rac1 activation. Mice with stromal or hematopoietic *Plxna4* deletion exhibited enhanced CTL infiltration and impaired tumor growth. In a melanoma model, adoptive transfer of CTLs lacking *Plxna4* prolonged survival and improved therapeutic outcome, which was even stronger when combined with anti-PD-1 treatment. *PLXNA4* abundance in circulating CTLs was augmented in melanoma patients versus healthy volunteers but decreased after the first cycle of anti-PD-1, alone or in combination with anti-CTLA-4, in those patients showing complete or partial response to the treatment. Altogether, our data suggest that PlexinA4 acts as a “checkpoint”, negatively regulating CTL migration and proliferation through cell autonomous mechanisms independent of the interaction with host-derived PlexinA4 ligands semaphorins. These findings pave the way towards PlexinA4-centric immunotherapies and propose PlexinA4 detection in circulating CTLs as a potential way to monitor the response to immune checkpoint blockade in metastatic melanoma patients.

## **Synopsis**

Knocking out *PlexinA4* promotes CTL proliferation and infiltration into the lymph nodes and tumor bed, boosting anti-tumor immunity of endogenous or adoptively transferred T cells. *PLXNA4* downregulation in melanoma patient circulating CTLs is associated with response to ICIs.

## **Introduction**

Immunotherapy has emerged as a promising treatment for advanced cancer patients. Immune system-based cancer therapies offer a durable clinical benefit, because, they can potentiate a self-propagating and adaptable response once the immune system is activated (1). However, only a fraction of patients responds to such treatment (2). Most of the immunotherapy-resistant tumors are “cold”, entailing a severely impaired presence and activation status of effector T cells within the tumor microenvironment (TME) (3). Thus, understanding the mechanisms underlying T-cell exclusion could translate into a broader and more durable response to this therapeutic option.

Cytotoxic CD8<sup>+</sup> T lymphocytes (CTLs) are one of the most powerful anti-tumor cells in the TME and their infiltration in tumors correlates with good prognosis in several tumor types (4). Immune checkpoint inhibitors (ICIs) take advantage of these cells and their killing capacity, but these require both the presence and physical contact between anti-tumor T cells and cancer cells (1). Given the lack of pre-existing CTLs in T-cell “cold” tumors, it is very unlikely that the use of currently approved ICIs will lead to robust anti-tumoral T-cell responses in these tumor-types (5). Hence, priming of the tumor via a combination of different therapies might be used in order to recruit a higher number of CTLs into these tumors.

Plexins are large transmembrane glycoproteins that, in most cases, function as the receptors for semaphorins (6). In the nervous system, these proteins play a bifunctional role, having the capacity to exert both repulsive and attractive effects in neuronal wiring during development (7). Their ability to modulate the immune response in both physiological and pathological conditions (8) and their role as “cell positioning cues” within the TME have also been explored (9). Targeting plexin signals (or semaphorins) is therefore a promising therapeutic strategy to restore anti-tumor immunity.

PlexinA4 (PlxnA4) is a member of class A plexins (10), which interacts with Sema6A and Sema6B (11). When in association with neuropilin-1 (NRP1), it can also function as a co-receptor for Sema3A (12). In the central nervous system, PlxnA4 mediates axon repulsion by the direct binding to Sema6A and Sema6B (13,14). In the immune system, PlxnA4 has been implicated in macrophage Toll-like receptor (TLR)–mediated signaling and cytokine production in sepsis (15), anti-inflammatory polarization in colitis (16), and entry into hypoxic niches in cancer (17). In T cells, PlxnA4 negatively regulates T cell–mediated immune responses, with *Plxna4*-deficient mice showing exacerbated disease in a mouse model of experimental autoimmune encephalomyelitis (EAE) (18). Based on these findings, we defined the function of PlxnA4 in the control of the immune response in the context of cancer.

## **Materials and Methods**

### **Animals**

*Plxna4*-KO mice on a C57BL/6 background were obtained from Dr. Castellani (Institut NeuroMyoGène, Université de Lyon, France). C57BL/6 mice were purchased from Charles River. OT-I mice were purchased from Taconic. *Sema6a*-KO mice on a C57BL/6 background were obtained from Prof. Dr. Pasterkamp (Dept. of Translational Neuroscience, University Medical Center Utrecht, The Netherlands). All mice were used between 6 and 12 weeks old, without specific gender selection. In all experiments, littermate controls were used. Euthanasia was performed by cervical dislocation. Housing conditions and all experimental animal procedures were approved by the Animal Ethics Committee of the KU Leuven.

### **Bone marrow transplantation**

6-week-old C56BL/6 recipient mice were lethally irradiated with a dose of 9.5 Gy using the Small Animal Radiation Research Platform (SARRP, XSTRAHL). Femur and tibia bones were collected from donor mice of the appropriate genotype. In a sterile culture hood, bone marrow (BM) cells were obtained by flushing the bones with a syringe filled with RPMI 1640 medium (Gibco, Thermo Fisher Scientific, 21875034) supplemented with 10% heat-inactivated Fetal Bovine Serum (FBS, Biowest, S1810). The cells were subsequently filtered using a 40- $\mu$ m pore sized mesh and centrifuged for 5 minutes at 200  $\times$ g. BM cells were counted and  $10 \times 10^6$  cells were injected intravenously (i.v.) via tail vein in the irradiated recipient mice. Tumor experiments were initiated 6 to 8 weeks after bone marrow reconstitution. Red and white blood cell count was determined using a hemocytometer on peripheral blood, collected in heparin with capillary pipettes by retro-orbital bleeding.

### **Cell lines**

Murine Lewis Lung Carcinoma cells (LLC) and B16F10 melanoma cells were obtained from the American Type Culture Collection (ATCC). E0771 medullary breast adenocarcinoma cells were obtained from CH3Biosystems. All cells were cultured in DMEM medium (Gibco, Thermo Fisher Scientific, 41965039) supplemented with 10% heat-inactivated FBS, 2 mM glutamine (Gibco, Thermo Fisher Scientific, 25030024), 100 units/ml penicillin and 100  $\mu$ g/ml streptomycin (Gibco, Thermo Fisher Scientific, 15140122) at 37°C in a humidified atmosphere containing 5% CO<sub>2</sub>. For the overexpression of ovalbumin (OVA), the following plasmid was used: pCDH\_CMV7-OVA-EFI-G418. LLC and B16F10 cancer cells were transduced with concentrated lentiviral vectors and further selected with G418 antibiotics (1 mg/ml, Invivogen,

ant-gn) to generate a homogenous population of OVA-overexpressing cancer cells (LLC-OVA and B16F10-OVA). Overexpression of the OVA protein was confirmed by western blot. All cell lines were tested for mycoplasma and passaged in the laboratory for no longer than 6 months after receipt.

### **Tumor models**

Adherent growing murine cells,  $1 \times 10^6$  LLC and  $5 \times 10^5$  B16F10, were injected subcutaneously for LLC and orthotopically for B16F10 at the right side of the mouse in Phosphate-Buffered Saline (PBS, Gibco, Thermo Fisher Scientific, 14190094). Alternatively,  $5 \times 10^5$  E0771 medullary breast adenocarcinoma cells were injected orthotopically in the mammary fat pad of the second nipple on the right side in a volume of 50  $\mu$ l PBS. Tumor volumes were measured three times a week with a caliper and calculated using the formula:  $V = \pi \times d^2 \times D/6$ , where  $d$  is the minor tumor axis and  $D$  is the major tumor axis. At the end stage, tumors were weighed and collected for immunofluorescence and/or flow cytometric analyses. For survival analysis, a tumor volume of 1800  $\text{mm}^3$  was used as the humane endpoint.

### **Histology and immunostainings**

Tumors and lymph nodes (LNs) were collected and fixed in 4% formaldehyde (37% stock, VWR, ACRO119690250) diluted in PBS overnight at 4°C, dehydrated and embedded in paraffin. Serial sections were cut at 7  $\mu$ m thickness with an HM 355S automatic microtome (Thermo Fisher Scientific). Paraffin slides were first rehydrated to further proceed with antigen retrieval in Target Retrieval Solution, Citrate pH 6.1 (DAKO, Agilent, S1699). If necessary, 0.3% hydrogen peroxide (Stock 30%, Millipore, 1072090250) was added to methanol (VWR, 20848.320), to block endogenous peroxidases. The sections were blocked with the appropriate serum (DAKO, Agilent), matching the species of the secondary antibody, and incubated overnight at room temperature (RT) with the following antibodies: rat anti-CD8 $\alpha$  (Thermo Fisher Scientific, 4SM15, 1:100), rat anti-CD4 (Thermo Fisher Scientific, 4SM95, 1:100), rat anti-F4/80 (AbD Serotec, MCA497, 1:100), rabbit anti-FITC (AbD Serotec, 4510-7604, 1:200), rat anti-CD31 (BD Pharmingen, 550274, 1:50), rat anti-CD34 (BD Pharmingen, 553731, 1:100), Rabbit anti-NG2 (Millipore, AB5320, 1:200) and rat anti-PNAd (Biolegend, MECA-79, 1:100). Appropriate secondary antibodies raised against the species of the primary antibody were used: Alexa 488 (Molecular Probes, A21208, 1:200), 647 (Molecular Probes, A31573, 1:100) or 568-conjugated secondary antibodies (Molecular Probes, A11077, 1:200), biotin-labelled antibodies (Jackson ImmunoResearch, 711-065-152 and 712-065-153, 1:300) and,

when necessary, TSA Plus Cyanine 3 and Cyanine 5 System amplification (Perkin Elmer, Life Sciences, NEL744001KT and NEL745001KT, 1:50) were performed according to the manufacturer's instructions. Hoechst-33342 solution (Thermo Fisher Scientific, H3570, 1:1000) was utilized to visualize nuclei. Mounting of slides was done with ProLong Gold mounting medium without DAPI (Invitrogen, P36930). Imaging and microscopic analysis was performed with an Olympus BX41 microscope and CellSense imaging software.

### **Tumor hypoxia assessment and tumor perfusion**

Tumor hypoxia was detected 1 hour after intraperitoneal (i.p) injection of 60 mg/kg pimonidazole hydrochloride (Hypoxyprobe kit, Chemicon, HP3-100Kit) in LLC tumor-bearing mice. Tumors were harvested and fixed in 4% formaldehyde overnight. To detect the formation of pimonidazole adducts, 7  $\mu$ m thick sections were immunostained with rabbit anti-hypoxyprobe monoclonal (Hypoxyprobe kit, Chemicon, HP3-100Kit, 1:100) following the manufacturer's instructions. Perfused tumor vessels were counted on tumor sections from mice injected i.v. with 0.05 mg FITC-conjugated lectin (*Lycopersicon esculentum*; Vector Laboratories, B-1175-1).

### **Flow cytometry**

Mice were sacrificed by cervical dislocation, and tumors, livers, blood, LNs (inguinal and axillary LNs) or the tumor-draining LN (TdLN; the closest LN draining the tumor bed) were collected. Tumors were minced in  $\alpha$ MEM medium (Lonza, BE12-169F), containing 50  $\mu$ M  $\beta$ -mercaptoethanol (Gibco, Thermo Fisher Scientific, 21985023), 5 units/ml Deoxyribonuclease I 0,85 mg/mL (Roche, 10104159001), Collagenase V (Sigma-Aldrich, C9263-1G), 1,25 mg/mL Collagenase D (Roche, 11 088 882 001) and 1 mg/ml Dispase (Gibco, Thermo Fisher Scientific, 17105-041), and incubated in the same solution for 30 minutes at 37°C. Livers were processed in RPMI 1640 medium, supplemented with 10 units/ml Deoxyribonuclease I 0,85 mg/mL (Roche, 10104159001) and 120 units/ml Collagenase III (Worthington Biochemical, LS004182), using the gentleMACS™ dissociator (Miltenyi Biotec). The digested tissues were filtered using a 70- $\mu$ m pore sized mesh and cells were centrifuged 5 minutes at 300  $\times$ g. Blood samples were collected in heparin with capillary pipettes by retro-orbital bleeding. Red blood cell lysis was performed by using a home-made red blood cell lysis buffer (150 mM NH<sub>4</sub>Cl, 0.1 mM EDTA, 10 mM KHCO<sub>3</sub>, pH 7.4). LNs were processed on a 40- $\mu$ m pore cell strainer in sterile PBS and cells were centrifuged for 10 minutes at 300  $\times$ g. Red blood cell lysis was performed by using Hybri-Max™ (Sigma-Aldrich, R7757). Single cells were resuspended in

FACS buffer (PBS containing 2% FBS and 2 mM EDTA) and incubated for 15 minutes with Mouse BD Fc Block purified anti-mouse CD16/CD32 (BD-Pharmingen, 553142). Extracellular staining was performed for 30 minutes at 4°C. When necessary, permeabilization was performed using the eBioscience™ Fcγ3 / Transcription Factor Fixation/Permeabilization kit (Thermo Fisher Scientific, 00-5521-00) according to the manufacturer's instructions and cells were incubated overnight at 4°C with the intracellular antibodies. All antibodies used are described in Table S1. Cells were subsequently washed and resuspended in FACS buffer before flow cytometric analysis by a FACS Canto II, Fortessa X-20 or flow sorting by a FACS Aria III, Aria Fusion (BD Biosciences). Data was analyzed by FlowJo (TreeStar, Version 10.7). FMO (Fluorescence Minus One) controls were utilized in order to ensure proper gating of positive populations.

### **Mouse T-cell isolation and activation**

Naïve mouse T cells were isolated from the spleen, inguinal and axillary LNs. In brief, tissues were processed on a 40-µm pore cell strainer in sterile PBS and cells were centrifuged for 10 minutes at 300 xg. Red blood cell lysis was performed using Hybri-Max™. Total splenocytes were cultured in T-cell medium [RPMI 1640 medium supplemented with 10% heat-inactivated FBS, 100 units/ml penicillin and 100 µg/ml streptomycin, 1% MEM Non-Essential Amino Acids (NEAA, Gibco, Thermo Fisher Scientific, 11140035), 25 µM β-mercaptoethanol and 1 mM Sodium Pyruvate (Gibco, Thermo Fisher Scientific, 11360070)] at 37°C in a humidified atmosphere containing 5% CO<sub>2</sub>.

According to the experimental requirements, T cells were activated for 3 days by adding mouse anti-CD3/CD28-coated Dynabeads™ (Thermo Fisher Scientific, 11453D) at a 1:1 bead-to-cell ratio. At day 3 of activation, the beads were magnetically removed and activated T cells were further expanded for a maximum of 3 additional days in the presence of 10 ng/ml recombinant murine IL-2 (mIL-2, PeproTech, 212-12). CD8<sup>+</sup> T cells were isolated by using MagniSort™ Mouse CD8<sup>+</sup> T cell negative selection kit (eBioscience™, Thermo Fisher Scientific, 8804-6822-74) according to the manufacturer's instructions. CD4<sup>+</sup> T cells were isolated by using MACS™ mouse CD4<sup>+</sup> T Cell Isolation Kit (Miltenyi Biotec, 130-104-454) according to the manufacturer's instructions. According to the experimental requirements, activated T cells (at day 3 of stimulation) were treated for 48 hours with 15 µg/ml anti-PD-1 (RMP1-14, Biolegend) or the appropriate isotype control. FOXO inhibition in activated T cells at day 3 of stimulation

was performed by 48 hours of treatment with 80  $\mu$ M Carbenoxolone (CBX, Sigma-Aldrich, C4790) or the DMSO vehicle control (Dimethyl sulfoxide, Sigma, D2438).

### **Human T-cell isolation and activation**

Buffy coat samples from healthy donors were obtained from the Red Cross-Flanders. Human CD4<sup>+</sup> and CD8<sup>+</sup> T cells were directly isolated by using the StraightFrom™ Buffy Coat CD4 and CD8 MicroBead kit (Miltenyi Biotec, 130-114-980 and 130-114-978 respectively) according to manufacturer's instructions. Red blood cell lysis was performed using Hybri-Max™. T cells were activated in T cell medium for 3 days by adding human anti-CD3/CD28 coated Dynabeads™ (Thermo Fisher Scientific, 11132D) at a 1:1 bead-to-cell ratio. At day 3 of activation, the beads were magnetically removed and activated T cells were further expanded for a maximum of 7 additional days in the presence of 10 ng/ml recombinant human IL-2 (hIL-2, PeproTech, 200-02). According to the experimental requirements, activated T cells (at day 7 of stimulation) were treated for 48 hours with 15  $\mu$ g/ml anti-PD-1 (J116, BioXCell) or the appropriate isotype control.

### **Cytospin staining**

CD8<sup>+</sup> T cells and peripheral blood leukocytes were seeded onto glass slides by cytopspin centrifugation and fixed in 4% formaldehyde for 10 minutes, followed by incubation with 0.2% Triton-X (VWR, 1.086.031.000) diluted in PBS for 15 minutes. To reduce the immune background, sections were blocked with 10% donkey serum (Sigma, D9663) in PBS for 1 hour, followed by blocking with FAB fragment anti-mouse IgG (Jackson ImmunoResearch, 715-007-003, 1:10) for 1 hour. Samples were then probed overnight with mouse anti-PlexinA4 (R&D, 707201, 1:500) and incubated with Donkey Alexa 568-conjugated secondary antibodies (Molecular Probes, A10037, 1:100) for 45 minutes. Nuclei were counterstained with Hoechst-33342 and mounting of the slides was performed with ProLong Gold mounting medium without DAPI. All steps were performed at RT. Microscopy was conducted with an Olympus BX41 microscope and CellSense imaging software.

### **Quantitative RT-PCR**

RNA was extracted from T cells using the TRIzol™ reagent (Life Technologies, 15596018) according to the manufacturer's instructions. Reverse transcription to cDNA was performed with the SuperScript™ III First Strand cDNA Synthesis Kit (Life Technologies, 18080051) according to the manufacturer's instructions. Pre-made assays were purchased from Integrated DNA Technologies. The cDNA, primer/probe mix and TaqMan™ Fast Universal PCR Master

Mix were prepared according to manufacturer's instructions (Applied Biosystems, 4352042). Samples were loaded into an optical 96-well Fast Thermal Cycling plate (Applied Biosystems) and qRT-PCR was performed using a QuantStudio 12K Flex Real-Time PCR System (Applied Biosystems). Samples were run in technical duplicates. Data was normalized to housekeeping gene expression (*Hprt* for mouse and *TBP* for human genes). The commercially available probes (Integrated DNA technologies) used are listed in Table S2.

### **LCMV-OVA model**

WT mice were pre-conditioned by i.v. injection of  $1 \times 10^4$  naïve OT-I T cells. 24 hours later, the mice were vaccinated i.p. with  $10^5$  plaque-forming units (PFU) of a recombinant lymphocytic choriomeningitis virus expressing ovalbumin (LCMV-OVA; a kind gift from Prof. Dr. Daniel Pinschewer, University of Basel, Switzerland), as described in Flatz *et al.* (19). 7 days after LCMV-OVA infection, OT-I T cells were FACS sorted from the blood.

### **T-cell proliferation assay**

To monitor cell proliferation, activated T cells were labelled with 3.5  $\mu$ M Violet Cell Tracer (Thermo Fisher Scientific, C34557) at 37°C for 20 minutes. The cells were subsequently washed with FACS buffer and cultured according to the experimental requirements. Absolute numbers of T cells in culture were counted by flow cytometry using Precision Count Beads™ (Biolegend, 424902). According to the experimental requirements, activated T cells (at day 3 of stimulation) were treated with 100  $\mu$ M Rac1 inhibitor NSC23766 (Selleckchem, S8031) or the DMSO vehicle control.

### **Annexin V / PI apoptosis assay**

Activated CD8<sup>+</sup> T cells were collected, washed and resuspended in 100  $\mu$ l Annexin V Binding Buffer (Biolegend, 422201) containing 4  $\mu$ l of Annexin V (Biolegend, 640941) and 0.1  $\mu$ l Propidium iodide solution (1 mg/ml stock, Sigma Aldrich, P4864). After 15 minutes of incubation at RT, samples were analyzed by flow cytometry.

### **Transwell migration assay**

Migration of T cells was assessed by using transwell permeable supports with 5- $\mu$ m polycarbonate membrane (Costar, 3387). To determine cell migration in response to soluble factors, the lower chamber was loaded with 0.1% FBS, 200 ng/ml CCL21 (Peprotech, 250-13), 200 ng/ml CCL19 (Peprotech, 250-27B), 150 ng/ml CXCL9 (Peprotech 250-18) or 50 ng/ml CXCL10 (Peprotech, 250-16) in T-cell medium. T cells were incubated for 2 (naïve) or 3 hours

(activated) at 37°C and migrated cells in the bottom chamber were collected and counted by flow cytometry using Precision Count Beads™. According to the experimental requirements, activated T cells were pre-treated for 1 hour with 10 µg/ml anti-CCR7 (R&D, 4B12), 250 µg/ml anti-CXCR3 (Biolegend, CXCR3-173), 100 µM Rac1 inhibitor NSC23766 or the appropriate isotype or vehicle control.

### **LN homing assay**

Naïve CD8<sup>+</sup> T cells were isolated from WT and *Plxna4*-KO mice and labelled with either 3.5 µM Violet Cell Tracer or 1 µM carboxyfluorescein succinimidyl ester Cell Tracer (CFSE; Thermo Fisher Scientific, C34554). For CFSE labelling, cells were stained in PBS for 8 minutes at RT with gentle agitation. To label cells with Violet Cell Tracer, the staining was conducted for 20 minutes at 37°C with gentle agitation. Afterwards, a brief wash with complete RMPI medium was performed to quench any remaining dye. Healthy WT mice were injected i.v. with a 1:1 mixture between 1-2x10<sup>6</sup> labelled WT and *Plxna4* KO T cells. After 2 hours, LNs of the recipient mice were harvested and analyzed by immunohistochemistry and/or flow cytometry.

### **Tumor homing assay**

OT-I T cells were isolated from transgenic WT and *Plxna4*-KO OT-I mice, generated by the intercross of *Plxna4* heterozygous mice with OT-I positive mice. These mice have a monoclonal population of naïve TCR transgenic CD8<sup>+</sup> T cells (OT-I T cells) that recognize the immunodominant cytosolic chicken ovalbumin (OVA) “SIINFEKL” peptide. For activation of OT-I T cells, total splenocytes from OT-I mice were isolated and cultured for 3 days in T-cell medium with 1 µg/ml SIINFEKL peptide (IBA - LifeSciences, 6-7015-901) and 10 ng/ml mIL-2. At day 3 of activation, OT-I T cells were further expanded for a maximum of 3 additional days in the presence of 10 ng/ml mIL-2.

For the tumor homing assay, activated WT and *Plxna4* KO OT-I T cells were labelled with either 3.5 µM Violet Cell Tracer or 1 µM CFSE and injected i.v. with a 1:1 mixture between 2-3x10<sup>6</sup> WT and *Plxna4* KO OT-I T cells into WT recipient mice with established B16F10-OVA or LLC-OVA tumors. The tumors of recipient mice were harvested 24 and 48 hours after T-cell transfer and analyzed by flow cytometry.

### **Liver homing assay**

WT mice received a plasmid DNA by hydrodynamic injection (HDI). Each mouse was injected rapidly (<8 s) in the tail vein with 40 µg of pcDNA3 empty vector (EV) or pcDNA3-OVA (OVA) diluted in PBS in an injection volume of 10% of the body weight. 4 days after HDI,

activated WT and *Plxna4* KO OT-I T cells were labelled with either 3.5  $\mu$ M Violet Cell Tracer or 1  $\mu$ M CFSE and injected i.v. with a 1:1 mixture between 2-3x10<sup>6</sup> WT and KO OT-I T cells into mice. 24 hours after T-cell transfer, blood and livers were harvested and analyzed by flow cytometry.

### **Plasmids and lentiviral vectors**

In the overexpression experiments, the following plasmids were used: pCDH-CMV-Sema3a-DYK-EF1-Puro (*Sema3a* OE), pCDH-CMV-Sema6a-DYK-EF1-Puro (*Sema6a* OE), pCDH-CMV-Sema6b-DYK-EF1-Puro (*Sema6b* OE) and pCDH-CMV-MCS-EF1-Puro (EV). B16F10-OVA cancer cells were transduced with concentrated lentiviral vectors and further selected with puromycin antibiotics (1  $\mu$ g/ml, Sigma, P9620) to allow the generation of a homogenous population of overexpressed (and empty vector control) cancer cells.

### **GTPase Pull down assay**

Rac1 and Rap1 activation were measured by using a Rac1 or Rap1 activation assay kit (Thermo Fisher Scientific, 16118 and 16120 respectively) according to the manufacturer's instructions. Briefly, cell lysis was performed by incubating activated T cells (at day 5 of stimulation) with the lysis buffer for 5 minutes on ice. The lysates were centrifuged for 15 minutes at 16,000 xg and subsequently incubated with the glutathione S-transferase (GST)-fused with *i*) p21-binding domain of Pak1 (GST-Pak1-PBD, 20  $\mu$ g) or *ii*) RalGDS-binding domain of Rap1 (GST-RalGDS-RBD, 20  $\mu$ g), bound to glutathione resin at 4°C for 60 minutes with gentle rocking. After being washed three times with lysis buffer, the samples were eluted in 2x SDS reducing sample buffer and analyzed for bound Rac1 (GTP-Rac1) or Rap1 (GTP-Rap1) by western blot.

### **Western blotting**

Protein extraction of liver samples was performed by using a home-made RIPA lysis buffer (50 mM Tris HCl pH 8, 150 mM NaCl, 1% Triton X-100, 0.5% sodium deoxycholate, 0.1% SDS) supplemented with Complete Protease Inhibitor Cocktail (Roche, 11697498001) and PhosSTOP™ phosphatase inhibitor (Roche, 04906837001). Lysates were incubated on ice for 30 minutes before centrifuging 15 minutes at 4°C to remove cellular debris. Protein concentration of cell extracts was determined by using Pierce™ bicinchoninic acid (BCA) reagent (Thermo Fisher Scientific, 23227) according to the manufacturer's instructions. Protein samples were denatured by adding a home-made 6X loading buffer ( $\beta$ -mercaptoethanol 0,6 M; SDS 8%; Tris-HCl 0,25 M pH 6,8; glycerol 40%; Bromophenol Blue 0,2%), incubated at 95°C for 5 minutes. Samples containing equivalent amounts of protein were subjected to 12%

SDS-polyacrylamide gel electrophoresis. Proteins were transferred onto a nitrocellulose membrane using the Trans-Blot Turbo™ Transfer System (Bio-Rad) according to manufacturer's instructions. The membranes were blocked for non-specific binding in 5% non-fatty dry milk (Cell Signaling, 9999S) in home-made Tris Buffered Saline-Tween 0.1 % (50 mM Tris HCl pH 7.6, 150 mM NaCl, 0.1% Tween; TBS-T) for 1 hour at RT and incubated with primary antibody overnight at 4°C. The following antibodies were used: mouse anti-Rac1 (Thermo Fisher Scientific, 16118, 1:1000), rabbit anti-Rap1 (Thermo Fisher Scientific, 16120, 1:1000) and mouse anti-Vinculin (Sigma-Aldrich, V9131, 1:200), mouse anti-Ovalbumin (Abcam, ab17293, 1:500). After incubation with the primary antibodies, the membranes were washed for 15 minutes in TBS-T and incubated with the appropriate secondary antibody (1:5000 in 5% non-fatty dry milk in TBS-T) for 1 hour at RT. The following secondary antibodies were used: goat anti-mouse and goat anti-rabbit IgG-HRP (Santa Cruz biotechnology, sc-2005 and sc-2004 respectively). The signal was visualized with Enhanced Chemiluminescent Reagents (ECL; Invitrogen, WP20005) or SuperSignal™ West Femto Chemiluminescent Substrate (Thermo Fisher Scientific, 34094) with a digital imager (ImageQuant LAS 4000, GE Health Care Life Science Technologies). The results of the GTPase pulldown assay were normalized against the corresponding band of the total proteins.

### **Adoptive T-cell transfer**

ACT experiments were performed with either naïve or activated OT-I T cells. WT recipient mice carrying subcutaneous LLC-OVA or orthotopic B16F10-OVA tumors (average tumor size of 30-50 mm<sup>3</sup>) were injected i.v. with either PBS, 1-3x10<sup>6</sup> WT or the same number of *Plxna4* KO OT-I T cells. Starting from the day of ACT, recipient mice were injected daily i.p. with 5 µg/mouse of recombinant human IL-2 in a volume of 200 µl of PBS for 4 consecutive days. Recipient mice were additionally treated i.p. 3 times per week with 10 mg/kg anti-PD-1 (RMP1-14, Biolegend) or the appropriate isotype control, starting from an average tumor size of 200 mm<sup>3</sup>. The tumors were measured every day and were weighted and collected at the end stage for flow cytometric analysis.

### **Human samples**

Blood samples were freshly collected from metastatic melanoma patients before and 3 weeks after the first cycle of ICI therapy (anti-PD-1 alone or in combination with anti-CTLA-4). Response assessment of melanoma patients with stage III and IV non-resectable disease was performed as per response evaluation criteria in solid tumors (RECIST v1.1) (20). Patients with complete or partial responses were categorized as responders, while non-responders only

achieved stable or progressive disease as their best overall response. Patients with resectable stage III disease all underwent complete LN dissection, which coincided with the “on-treatment” sampling time point. Pathological response was assessed on the resection specimen. Patients with a complete response were categorized as responders, while patients without pathological complete response were categorized as non-responders. All relevant clinicopathological information of the human subjects is provided in Table S3. Inclusion and exclusion criteria for the study can be found in Table S4. The research using human samples was conducted according to institutional and European Union ethical standards, and all subjects ensured written informed consent to participate in this study.

In brief, peripheral blood mononuclear cells from patients and healthy volunteers were immediately isolated by density gradient centrifugation using Lymphoprep™ (Stemcell, 07811). CD4<sup>+</sup> and CD8<sup>+</sup> T cells were negatively selected using MojoSort™ Human CD4 and CD8 T Cell Isolation Kit (Miltenyi Biotec, 480010 and 480129 respectively), according to manufacturer’s instructions. For the expression analysis of circulating monocytes, cDNA samples from patients with different tumor types and age-matched healthy controls (Table S5) were provided by the “Monomark” clinical study (21).

## **Statistics**

Data entry and all analyses were performed in a blinded fashion. All statistical analyses were performed using GraphPad Prism software (Version 9.2). Pairwise comparisons on two experimental conditions were performed using an unpaired Student’s t-test or a paired t-test for competition assays. Grouped data were assessed by two-way ANOVA with Bonferroni’s multiple comparison correction. Survival curves were compared with the log-rank (Mantel-Cox) test. Statistical details of the experiments can be found in the figure legends. Detection of mathematical outliers was performed using the Grubbs’ test in GraphPad. Sample sizes for all experiments were chosen based on previous experiences. All graphs show mean values ± SEM.

## **Results**

### **Genetic knockout of *Plxna4* in the stroma inhibits tumor progression and increases CTL infiltration**

To study the role of PlxnA4 in the TME, we took advantage of *Plxna4* knockout (KO) mice (22) (Figure S1A). Compared to wild type controls (WT), *Plxna4* KO mice were phenotypically identical and had similar blood counts (Table S6). By implanting LLC cancer cells

subcutaneously, we observed a significantly slower tumor growth in *Plxna4* KO versus WT mice (Figure 1A and 1B). Since previous experiments with human umbilical vein endothelial cells (HUVECs) have shown the involvement of PLXNA4 in basic fibroblast growth factor (bFGF)-induced angiogenic signaling (23), we analyzed tumor blood vessel parameters in WT and *Plxna4* KO mice. Tumor vessel density, perfusion and pericyte coverage were comparable between WT and *Plxna4* KO mice (Figure S1B-D), resulting in no differences in tumor hypoxic areas (Figure S1E). PlxnA4 was also reported to be part of the signaling complex involved in the positioning of tumor-associated macrophages (TAMs) inside hypoxic niches (17). However, we could not observe any difference in either TAM infiltration (Figure S1F) or localization within hypoxic regions (Figure S1G and S1H). Additionally, gene expression markers typically used to characterize classically (M1-like) and alternatively activated (M2-like) macrophages were unaltered in sorted TAMs from WT and *Plxna4* KO tumor-bearing mice (Figure S1I), suggesting that, at least in these conditions, *Plxna4* is not required for macrophage localization or polarization within the TME.

PlxnA4 was described as a negative regulator of T cell-mediated immune responses (18,24), so we therefore investigated if the tumor-suppressing phenotype observed in *Plxna4* KO mice was related to T-cell functions. Flow cytometric analysis showed that tumor-bearing *Plxna4* KO versus WT mice had increased numbers of CTLs in the tumor-draining lymph nodes (TdLN) (Figure 1C and S1J). Histologically, we found that mice lacking *Plxna4* had increased infiltration of CTLs into the core of the tumor when compared to WT mice (Figure 1D). Paired analysis of CTLs in the outer area versus the inner area of the same tumor suggested that, compared to their WT counterparts, *Plxna4* KO CTLs had increased capacity of migrating from the outer rim into the core of the tumor (Figure 1E and 1F). Therefore, we hypothesized that *Plxna4* KO CTLs subvert a PlexinA4-dependent T-cell exclusion mechanism seen in WT mice. Consistently, in an orthotopic B16F10 melanoma model, we observed a higher infiltration of CTLs, in both the TdLN (Figure 1G) and primary tumor (Figure 1H) of *Plxna4* KO versus WT mice. When looking more closely into the different CD8<sup>+</sup> T cell subsets (naïve, central memory, effector/memory and terminally exhausted T cells), the proportion of each CD8<sup>+</sup> T cell subset in both the TdLN and tumors remained the same in *Plxna4* KO versus WT mice (Figure S1K and S1L). Conversely, in both tumor models, total CD4<sup>+</sup> T cells did not change, either in numbers (Figure S1M-P) or in their localization within the TME (Figure S1Q and S1R).

To further restrict the KO of PlxnA4 to the immune system, we generated bone marrow (BM) chimeras by transplanting BM cells from WT or *Plxna4* KO mice into lethally irradiated WT

recipient mice, WT→WT and *Plxna4* KO→WT, respectively. Upon reconstitution, *Plxna4* KO→WT chimeras displayed normal blood counts, comparable to those of WT→WT mice (Table S7). Upon subcutaneous engraftment, LLC tumor growth in *Plxna4* KO→WT chimeras was slower than in WT→WT chimeras (Figure 1I and 1J), resembling our results in *Plxna4* KO mice (Figure 1A and 1B). In an alternative tumor model, obtained by the orthotopic injection of E0771 breast cancer cells, tumor progression was significantly decreased upon deletion of *Plxna4* in the BM (Figure 1K and 1L). Similarly to *Plxna4* KO mice, higher numbers of CTLs, but not of CD4<sup>+</sup> T cells, were found in both the TdLN (Figure 1M and S1S) and primary tumor (Figure 1N and S1T) in *Plxna4* KO→WT compared to WT→WT chimeras. Altogether, these results show that a *Plxna4*-deficient tumor stroma or immune system results in impaired tumor growth and in the selective increase of CTLs inside both the TdLN and the tumor core.

### ***Plxna4* expression is dynamically regulated in CTLs**

Elevated CTL infiltration in the TME correlates with a good prognosis in several tumor types (4). Since we detected higher CTL numbers in the tumor core of *Plxna4* KO mice (Figure 1D, 1H and 1N), we investigated the direct role of *Plxna4* in these cells. Firstly, we observed that *Plxna4* expression was upregulated in activated CTLs upon 3 days of anti-CD3/CD28 stimulation *in vitro* (Figure 2A). Purified CD4<sup>+</sup> T cells showed similar kinetics of *Plxna4* expression, but at about one-third the abundance of CTLs, both in the naïve and active state (Figure 2A). In line with regulation at the transcript level, protein staining revealed that the number of PlxnA4-expressing activated CTLs was increased compared to naïve cells (Figure 2B). Similarly to murine data, the expression of *PLXNA4* in human T cells was also upregulated upon later stages of T-cell activation, and this to a greater degree in CTLs than in CD4<sup>+</sup> T cells (Figure 2C). Based on these observations, we characterized the expression of *Plxna4* in CTLs sorted from the circulation of healthy or tumor-bearing mice. Compared to healthy mice, *Plxna4* was upregulated in CTLs in both an orthotopic melanoma model (B16F10) and a subcutaneous LLC lung cancer model (Figure 2D). *Plxna4* was also upregulated in circulating CTLs after mouse infection with a lymphocytic choriomeningitis virus expressing the surrogate antigen ovalbumin (LCMV-OVA), which has a specific tropism for dendritic cells (Figure S2A) (19). These data suggest an involvement of PlxnA4 in CTLs upon antigen recognition.

To assess the relation between PlxnA4 expression, activation status and tissue of origin, we sorted different CD8<sup>+</sup> T cell subsets from the blood and LNs in healthy mice (Figure S2B), or from the blood, TdLN and tumor tissue in B16F10 tumor-bearing mice (Figure S2C). In healthy

mice, *Plxna4* was expressed in all the circulating T cell subsets, but it was decreased in effector/memory T cells or undetectable in naïve and central memory T cells sorted from the LNs (Figure 2E). In B16F10 tumor-bearing mice, *Plxna4* abundance in circulating naïve and central memory T cells were comparable to those measured in healthy mice but was strongly augmented in circulating effector/memory T cells, which have encountered the antigen in the TdLN and consequently express CD44 (Figure 2F). However, in the TdLN or in the tumor bed, *Plxna4* expression in effector/memory T cells was reduced and was undetectable in naïve, central memory and exhausted CTLs, the latter being the most abundant subset in the tumor bed (Figure 2F and S2C). Altogether, our data suggest that T-cell activation increases *Plxna4* in effector/memory CTLs, but this expression is downregulated in all T cell subsets when entering the inflammatory site. These observations held also true in a liver inflammation model, induced by hydrodynamic injection (HDI) of a plasmid directing the expression of ovalbumin (OVA) (25). In this model, circulating antigen-primed CD8<sup>+</sup>CD44<sup>Hi</sup> T cells expressed more *Plxna4* than their naïve CD44<sup>Lo</sup> counterparts (Figure 2G). Similarly to what observed in tumor-infiltrating CTLs (Figure 2F), *Plxna4* expression was also halved in CD8<sup>+</sup>CD44<sup>Hi</sup> T cells infiltrating inflamed livers (Figure 2G). Altogether, these data show that *Plxna4* expression is induced in effector/memory CTLs upon T-cell activation and sustained in circulation, while reduced at the inflammatory sites.

### **Genetic knockout of *Plxna4* in CTLs increases their motility and proliferation via enhanced Rac1 activity**

As the expression of *Plxna4* in circulating CTLs was increased in tumor-bearing mice compared to healthy mice, but decreased upon their infiltration into the tumor bed (Figure 2D and 2F), we studied the functional relevance of *Plxna4* in CTLs. We analyzed the proliferation of WT and *Plxna4* KO CTLs in an *in vitro* time course experiment. From day 3 of activation, *Plxna4* KO CTLs showed a higher proliferation rate than WT cells (Figure 3A, 3B and S3A). This difference in proliferation was increasing with time, reaching almost 2-fold higher at day 5 of stimulation (Figure 3A), consistent with the observation that *Plxna4* expression increases over time following stimulation (Figure 2A). In contrast, the apoptotic rate of WT and *Plxna4* KO CTLs at different timepoints following stimulation did not change (Figure S3B). Downstream effector functions of *in vitro* activated CTLs were also not affected, since the analysis of interferon- $\gamma$  (IFN $\gamma$ ) and granzyme B (GrzmB) expression did not show any differences between WT and *Plxna4* KO CTLs (Figure S3C-F). Unlike CTL proliferation, expansion of activated CD4<sup>+</sup> T cells did not change significantly between WT and *Plxna4* KO T cells (Figure S3G).

Given the increased numbers of *Plxna4* KO CTLs in the TdLN (Figure 1C, 1G and 1M) and in the primary tumor site (Figure 1D, 1H and 1N), we questioned whether chemotaxis could also be affected. *In vitro* transwell migration assays, in the presence of CCL21 and CCL19, chemokines involved in T-cell homing to the LNs (26), or CXCL9 and CXCL10, chemokines involved in T-cell homing to tumors (27), showed that *Plxna4* KO CTLs had increased migratory capacity than WT cells (Figure 3C and 3D), whereas CD4<sup>+</sup> T-cell migration did not change (Figure S3H). The surface abundance of the CCL21 and CCL19 receptor CCR7 in naïve CTLs, or the CXCL9 and CXCL10 receptor CXCR3 in activated CTLs, were comparable in both genotypes (Figure S3I and S3J). However, transwell migration assays with naïve CTLs, treated with anti-CCR7, and activated CTLs, treated with anti-CXCR3, demonstrated reduced migration of *Plxna4* KO CTLs (Figure 3E and 3F). This suggests that the increased migration potential of *Plxna4* KO CTLs is dependent on chemokine receptor signaling. Since the intracellular portion of PlxnA4 contains a GTPase activating protein (GAP) domain with a Rho GTPase-binding domain insert (28), and Rac1, a member of the Rho small GTPases family, is necessary for the correct homing of T cells to the LNs (29), we hypothesized that PlxnA4 could regulate the activation of small GTPases in CTLs. We performed a GTPase pull-down assay to measure GTP-bound Rac1 in both WT and *Plxna4* KO activated CTLs. Compared to WT, *Plxna4* KO T cells had an increased amount of active (GTP-bound) Rac1 (Figure 3G). The amount of GTP-bound Rap1, however, was similar between both conditions (Figure S3K and S3L). In line with the previously reported involvement of Rac1 in CTL migration and proliferation (30), pharmacologic Rac1 inhibition on activated CTLs was sufficient to reduce migration and proliferation of both *Plxna4* WT and KO cells (Figure 3H and 3I). The latter suggests that active Rac1 is required for the phenotype observed in *Plxna4* KO CTLs.

### ***Plxna4* KO CTLs show increased homing and proliferation capacity in inflammatory sites**

To assess the *in vivo* role of *Plxna4* on CTL migration and proliferation, we performed competition assays in which WT and *Plxna4* KO CTLs, either naïve (LN-homing) or *in vitro* pre-activated (inflamed tissue-homing), were co-injected i.v. into mice. When naïve WT and *Plxna4* KO CTLs were transferred into healthy WT mice, *Plxna4* KO CTLs were more efficient in reaching the LNs (Figure 4A-B and S4A-B). Both WT and *Plxna4* KO CTLs were able to enter the paracortical areas of the LNs without entrapment in the high endothelial venules (HEVs, Figure 4B). To evaluate whether increased detection of *Plxna4* KO CTLs was due an inability to exit the LNs, we treated WT mice with fingolimod (FTY720), an

immunomodulatory drug that inhibits lymphocyte egress from lymphoid tissues by downregulating sphingosine-1 phosphate receptor (S1PR) (31). Treatment with FTY720 entrapped both WT and *Plxna4* KO CTLs in the LNs, but *Plxna4* KO CTLs were still present in higher numbers in the LNs compared to WT controls (Figure 4C). To further investigate if *Plxna4* deficiency would affect T-cell egression from the LNs, we generated WT and *Plxna4* KO OT-I T cells, expressing a T-cell receptor (TCR) which specifically recognizes the OVA peptide presented in major histocompatibility complex (MHC) class I. Thereafter, we took advantage of the LCMV-OVA model, where infected dendritic cells present the OVA peptide in MHC class I (19). Following the systemic injection of naïve WT or *Plxna4* KO OT-I T cells in LCMV-OVA infected mice, we calculated the ratio between antigen-primed CD44<sup>Hi</sup> and naïve CD44<sup>Lo</sup> WT or *Plxna4* KO OT-I T cells in circulation over time. In this way, we found that similar numbers of CD44<sup>Hi</sup> *Plxna4* KO OT-I T cells were released into the blood 16 hours earlier than CD44<sup>Hi</sup> WT OT-I T cells but their speed of egression (graphically represented by the slope of the line) was the same (Figure 4D). This observation suggests that the exit from the LNs of activated *Plxna4* KO CTLs was not altered but only anticipated due to their faster arrival into the LN.

Next, we studied the biological functions of *Plxna4* in CTLs within the tumor or other sites of inflammation. In competition assays, we found increased tumor homing of *Plxna4* KO versus WT OT-I T cells 24 hours after their systemic co-injection in mice bearing OVA-expressing B16F10 (Figure 4E) or LLC tumors (Figure S4C). To differentiate if the increased number of *Plxna4* KO CTLs in the tumor was a consequence of increased migratory/infiltrative capacity or higher proliferative ability, as observed *in vitro* (Figure 3A-B), we followed OVA-expressing melanoma tumors for an additional 24 hours. Forty-eight hours after systemic injection of OT-I T cells, the ratio between *Plxna4* KO/WT OT-I T cells in the tumor bed was higher compared to what was calculated at 24 hours (Figure 4E and S4D), suggesting that the increased intratumoral accumulation of *Plxna4* KO CTLs was the result of both augmented migration and proliferation. The fluorescent probe labelling *Plxna4* KO tumor-infiltrating OT-I T cells was more diluted than in WT OT-I cells 24 hours after the systemic co-injection of activated WT and KO CTLs (Figure S4E), further suggesting a higher proliferation rate of *Plxna4* KO CTLs. To control for potential differential recruitment, we co-injected activated WT and *Plxna4* KO OT-I T cells intratumorally in B16F10-OVA tumors and observed increased proliferation in cells lacking *Plxna4* (Figure 4F). Then, we assessed if the loss of *Plxna4* could confer both a migratory and proliferative advantage in other inflammatory conditions as well. To this end,

we used the HDI model described above and found that *in vitro* activated *Plxna4* KO OT-I T cells infiltrated the inflamed livers more efficiently than WT OT-I T cells (Figure 4G). This effect was more evident when hepatocytes were forced to express OVA (Figure 4G and S4F-G), which would boost proliferation as well. Taken together, these results suggest that *Plxna4* deletion in CTLs increases both their migratory/infiltrative capacity and proliferation rate in response to TCR activation.

Finally, we evaluated whether infiltrating CTLs were attracted or repulsed by interactions *in trans* with semaphorins expressed in the TME. To this end, B16F10-OVA cancer cells overexpressing the most relevant PlxnA4 ligands (*Sema3a*, *Sema6a* or *Sema6b*) were injected in WT mice (Figure S4H-J). Consistent with our previous observations (Figure 4E), 24 hours after systemic injection, *Plxna4* KO OT-I T cells were more efficient in infiltrating melanoma tumors transduced with a mock empty vector (Figure 4H). This finding held true even when the tumors overexpressed *Sema3a*, *Sema6a* or *Sema6b* (Figure 4H). Moreover, the increased homing capacity of *Plxna4* KO versus WT OT-I T cells was also seen in *Sema6a* KO tumor-bearing mice (Figure 4I). Ruling out the engagement of *Sema6A* presentation by T cells themselves, activated *Sema6a* KO CTLs did not mimic *Plxna4* deficiency in terms of *in vitro* migration towards CXCL10, but rather showed the same chemotaxis as observed in WT cells (Figure S4K). Altogether, these findings suggest that presentation of semaphorins by the host (or autocrine signals by *Sema6A*) do not affect CTL infiltration and provide evidence for another non-conventional PlxnA4-dependent but semaphorin-independent mechanism controlling CTL motility in cancer.

### **Adoptive transfer of *Plxna4* KO CTLs shows improved anti-tumor efficacy in a melanoma model**

Prompted by our observations that PlxnA4 functions as a negative regulator of CTL proliferation and migration, we evaluated if the deletion of *Plxna4* in CTLs was sufficient to increase anti-tumor immunity in the context of adoptive T-cell transfer (ACT). As a proof-of-concept of immunotherapeutic validation of *Plxna4* deficiency in CTLs, we first injected naïve WT or *Plxna4* KO OT-I T cells i.v. into LLC-OVA lung and B16F10-OVA melanoma tumor-bearing WT recipient mice. Mice receiving *Plxna4* KO OT-I T cells displayed a higher degree of tumor inhibition (Figure S5A-B), pointing to a direct effect of *Plxna4* deficiency in CTL activity. Secondly, consistent with a therapeutic approach, activated OT-I T cells were transferred into the circulation of B16F10-OVA tumor-bearing WT recipient mice. In this

setting, *Plxna4* KO OT-I T cells exerted increased anti-tumor effects than their WT counterparts, as demonstrated by decreased tumor growth and weight (Figure 5A-C). As expected, WT CTLs were also able to control tumor growth, but to a lesser extent than *Plxna4* KO OT-I T cells (Figure 5A-C). When we analyzed the number of tumor-infiltrating CTLs 4 days after ACT, melanoma tumors that received *Plxna4* KO OT-I T cells contained an increased number of intratumoral OT-I T cells compared to the ones treated with WT OT-I cells (Figure 5D). Nevertheless, these cells showed no difference in cytotoxicity, evaluated by their expression of IFN $\gamma$  and GzmB after T-cell re-stimulation *ex vivo* (Figure S5C-D). In this model of ACT, the administration of *Plxna4* KO OT-I T cells also extended overall survival when compared to the adoptive transfer of WT OT-I T cells (Figure 5E). Taken together, these data demonstrate that *Plxna4* deletion in CTLs is sufficient to increase anti-tumor immunity in a conventional ACT setting and that targeting of PlexinA4 might thus be a valuable strategy to improve CTL infiltration.

### **Potential clinical relevance of *PLXNA4* in CTLs in melanoma patients**

To translate our findings to human cancer, we analyzed *PLXNA4* expression in circulating CTLs in a cohort of metastatic melanoma patients (Table S3). Similarly to our observations in a murine model (Figure 2), CTLs isolated from the peripheral blood of melanoma patients expressed higher quantities of *PLXNA4*, but not of other type-A plexins, compared to those measured in circulating CTLs from healthy donors (Figure 6A and S6A-C). *PLXNA4* abundance was also higher in circulating CD4<sup>+</sup> T cells isolated from the same patients (Figure S6D). In contrast, expression of *PLXNA4* in circulating monocytes isolated from both healthy volunteers and patients across different tumor types were low or undetectable (Figure S6E and Table S5).

We then analyzed *PLXNA4* expression in circulating CTLs of melanoma patients prior to and after the first cycle of ICI therapy (anti-PD-1 alone or in combination with anti-CTLA-4). We observed a significant decrease of *PLXNA4* in CTLs following treatment (Figure 6B). When stratifying these patients for their clinical response to ICI therapy, we found that the decrease in *PLXNA4* expression in circulating CTLs was significant in the responders but not in the non-responders (Figure 6C and 6D).

Based on these clinical data, we speculated that the benefit from ICI therapy may depend, at least partly, on the downregulation of PlexinA4. This hypothesis was tested by treating B16F10

tumor-bearing mice with anti-PD-1 for a week, resulting in a reduction of *Plxna4* expression in circulating CTLs compared to IgG-treated tumor-bearing mice (Figure 6E). This downregulation of *PLXNA4* expression upon anti-PD-1 blockade was also true for *in vitro* activated human CTLs, but not for CD4<sup>+</sup> T cells (Figure 6F). The hypothesis that PD-1 blockade acts partly, but not only, through the downregulation of *Plxna4* in CTLs was also suggested by our findings that anti-PD-1 therapy in combination with ACT of WT OT-I cells reached a similar extent of tumor inhibition as observed with the transfer of *Plxna4* KO OT-I T cells alone (Figure 6G). Perhaps by means of PlexinA4-unrelated mechanisms of anti-PD-1, such as unleashing the PI3K–Akt pathway (32), the combination of *Plxna4* KO OT-I ACT and anti-PD-1 therapy led to an even stronger reduction in tumor growth than with *Plxna4* KO OT-I ACT alone (Figure 6G). Members of the Forkhead box O (FOXO) family of transcription factors (TFs), which are activated downstream to PD-1 and upon persistent TCR stimulation (33,34), are described to regulate *Plxna4* expression (35). When treating *in vitro* activated CTLs with Carbenoxolone, an inhibitor of FOXO1, 3, 4 and 6 (36), we observed that *Plxna4* expression was reduced even further than upon anti-PD-1 treatment (Figure 6H), providing initial support that FOXO TFs may promote *Plxna4* expression upon chronic TCR stimulation and PD-1 induction.

## **Discussion**

In the last decade, immunotherapy has emerged as a promising therapeutic option for cancer patients. The use of ICIs, in particular, has revolutionized the field, enabling durable control of previously highly refractory and aggressive cancers, such as melanoma and lung cancer. However, a significant percentage of patients – 60% to 80% – still do not benefit from this strategy (37). One of the main factors hampering ICIs is the exclusion of CTLs from the tumor bed, making these tumors T-cell “cold”. In this study, we show that targeting PlexinA4 might represent a novel strategy to drive T-cell inflammation in T-cell non-enriched tumors. Our data show that PlexinA4 is dynamically regulated in CTLs and that its absence promotes an increased proliferative and homing capacity to the TdLN and the tumor bed, leading to a more effective anti-tumor response (Figure 6I).

In our study, *Plxna4* deletion in the stroma reduced tumor growth by specifically enhancing CTL infiltration, while the phenotype of other stromal cells remained unaffected. Although PlexinA4 was shown to play a role in macrophages in the context of cancer or other pathological conditions (15-17), we observed that deletion of *Plxna4* was not sufficient to impact on

macrophage localization and phenotype. PlxnA4 was also described as a negative regulator of CD4<sup>+</sup> T-cell immune responses in experimental autoimmune diseases (18,24). In our models, PlxnA4 is expressed by CD4<sup>+</sup> T cells but at lower abundance than in CTLs. Moreover, neither the infiltration nor the distribution of *Plxna4* KO CD4<sup>+</sup> T cells within the tumor was altered, pointing to a function of PlxnA4 specifically in CTLs. Given the functional redundancy among class A plexins (17,38), homologous receptors expressed in TAMs, CD4<sup>+</sup> T cells or endothelial cells, such as PlxnA1, could compensate for the absence of PlxnA4. In contrast, PlxnA4 is indispensable for the fine-tuning of CTL proliferation and migration.

In terms of expression, naïve T cells found in the LNs show undetectable transcription of *Plxna4* compared to circulating naïve T cells, suggesting that the downregulation of *Plxna4* is required for CTLs to enter the lymphoid tissue. Indeed, homing of naïve *Plxna4* KO CTLs towards LNs of healthy mice was increased compared to WT CTLs. Upon T-cell activation, *Plxna4* transcripts were upregulated in CTLs in tumors, as well as in experimental models of liver inflammation or viral infection, demonstrating that different microenvironmental signals associated with inflammation, infections or tumor progression can result in similar expression patterns, as previously described (39). In particular, PlexinA4 protein expression was increased in CTLs activated *in vitro* when compared to their naïve counterpart, suggesting that PlexinA4 is upregulated upon T-cell activation. Consistently, *Plxna4* transcription was specifically induced in the circulating effector/memory CTL fraction in tumor-bearing mice but reduced at inflammatory sites (cancer and liver), suggesting that *Plxna4* downregulation is required for their entry in these tissues. Indeed, genetic KO of *Plxna4* in activated CTLs increased their infiltration to both the tumor and the inflamed liver parenchyma. In addition, we hypothesized that higher *Plxna4* transcription observed in the pool of tumor-associated effector/memory T cells, compared to the undetectable levels in central memory and terminally exhausted T cells, was mainly reflecting the presence of PlxnA4<sup>High</sup> excluded T cells at the tumor border. In contrast, few PlxnA4<sup>low</sup> T cells enter the tumor core and proliferate when encountering tumor-associated antigens presented in MHC class I by the cancer cells or by tumor-infiltrating DCs (Figure 6I). In line with this idea, tumor-bearing mice with stromal or hematopoietic *Plxna4* deletion had increased CTL numbers in the tumor core, which is likely the result of improved infiltration and proliferation in response to antigen repriming (Figure 6I). This is also suggested by the fact that adoptive transfer of *in vitro* pre-activated *Plxna4* KO CTLs exhibit increased homing and proliferation within OVA-overexpressing tumors. Altogether, it is reasonable to speculate that PlxnA4 could work as a negative regulator of both naïve and effector/memory

CTLs, by breaking their recruitment into the LN and inflammatory sites. This mechanism is possibly mediated by the presence of pro-inflammatory, type I cytokines in these tissues (such as IL-10, IFN $\gamma$  or others), which counter this break in a dynamic process and promote the downregulation of *Plxna4* and thus the entry and the proliferation of naïve CTLs in the LNs, and effector/memory CTLs in the inflamed tissue. However, in the context of cancer, this process fails to occur completely, possibly because the TME is enriched in anti-inflammatory, type II cytokines which impede the downregulation of *Plxna4* in effector/memory CTLs that are thus excluded at the border of the tumor. The concept of PlexinA4 as a “break” of inflammatory processes agrees with previously published data showing that the absence of *Plxna4* exacerbates ongoing autoimmune diseases (18,24) but does not result *per se* in the spontaneous development of autoimmune disorders or other pathologies, since *Plxna4* KO mice appear to be healthy (18,22).

The intracellular portion of plexins contains GTPase-binding domains (28,40), which can interact and negatively regulate Rac1, a Rho family GTPase involved in the modulation of the cytoskeleton (30,41-43). Our data suggest that enhanced CTL migration in the absence of PlexinA4 might be due to increased activation of Rac1, since we observed that *Plxna4* deficiency was associated with augmented GTP-bound Rac1, in line with what has been shown before in *Plxna4*-silenced endothelial cells (23). The modulation of Rac1 by PlexinA4 is here functionally supported by the observation that treatment with the Rac1 inhibitor NSC23766 completely prevented the advantageous migration of *Plxna4* KO CTLs. Besides migration, CTL proliferation is also instrumental to mount a proper immune response (44). In this regard, *Plxna4* KO CTLs displayed increased proliferative capacity, arguing that PlexinA4 negatively regulates CTL proliferation as well, akin to what has been suggested for *Plxna4* KO CD4<sup>+</sup> T cells in the context of autoimmune diseases (18). This increased proliferation can be attributed to enhanced Rac1 activity as well (30), as supported by our *in vitro* data comparing *Plxna4* WT and KO CTLs treated with Rac1 inhibitors. However, future work is warranted to assess if direct or indirect mechanisms are enrolled by PlexinA4 to regulate Rac1 activation.

Given the repulsive activities propagated by PlexinA4 when interacting with semaphorins (13,14,45), it may be attractive to hypothesize that the exclusion of CTLs from the tumor bed is a consequence of repulsive cues. However, our data illustrate that the overexpression in cancer cells of the most relevant PlexinA4 ligands (Sema3A, Sema6A and Sema6B), or the expression of the high-affinity ligand Sema6A in the TME and by T cells themselves, does not

modulate CTL infiltration in the tumor bed. Since plexins are evolutionarily more conserved than semaphorins (46), we are tempted to believe that semaphorin-independent mechanisms are likely to be present in eukaryotic cells. Furthermore, we foresee that the inhibitory effect of PlxnA4 on CTL expansion and chemotaxis is cell autonomous, and therefore independent of the interaction *in trans* of PlexinA4 with semaphorins expressed in the TME. Of note, interactions *in cis* between plexins and transmembrane semaphorins, or other cell surface receptors, have been reported to modulate intracellular signaling and biological functions (45,47-49). Thus, currently unknown interactions of PlxnA4 with molecules co-expressed in T cells (other than Sema6A) could play a role in the observed phenotype, possibly by regulating Rac1 activation.

Our work suggests potential therapeutic and clinical implications. In an adoptive transfer setting, *Plxna4* KO CTLs outperformed WT cells in shrinking established B16F10 melanoma tumors, providing proof-of-concept that PlexinA4 targeting in CTLs facilitates anti-tumor immunity and could be integrated in existing cancer immunotherapy regimens. Since enforcing the trafficking of CTLs to malignant tissues can improve the efficacy of any immunotherapeutic regimens (50), and combination treatments are often needed to unleash a proper anti-tumor immune response (51), we believe that targeting PlexinA4 also holds the potential to act synergistically with conventional immunotherapies, including ICIs. In our preclinical tumor models, ACT with *Plxna4* KO CTLs in combination with anti-PD-1 led to a more potent anti-tumor immune response compared to monotherapy, demonstrating a potential clinical value of PlexinA4-targeted therapies. However, future studies should determine to which extent and with which implications on homeostatic immune control, the combined targeting of PlexinA4 and other inhibitory receptors on CTLs can further increase the anti-tumor immune response.

Supporting our preclinical data, *PLXNA4* expression was increased in circulating CTLs from metastatic melanoma patients compared to healthy controls, further strengthening a possible translation of our mechanistic and therapeutic conclusions to human disease. Moreover, *PLXNA4* expression in circulating CTLs was decreased after the first cycle of ICI therapy in melanoma patients that responded to the therapy. ICI therapy frequently leads to an increase in proliferation and migration of pre-existing CTLs (52,53), features related to the observed phenotype of *Plxna4* KO CTLs. This indicates that ICIs might partly work in circulation via the downregulation of PlxnA4 in CTLs separately from previously characterized mechanisms

(54). The expression of PD-1 (*Pdcd1*) is induced after TCR stimulation via members of the Nuclear factor of activated T-cells (NFAT) family of transcription factors (55). Upon persistent antigen stimulation, PD-1 signaling inhibits multiple TCR downstream pathways and FOXO TFs are activated, further promoting *Pdcd1* transcription (33). Consistent with *Plxna4* being upregulated as a late activation marker, FOXOs are essential for activated T cells within days following primary TCR activation (33,34). FOXOs are known to positively regulate several effector/memory functions such as T-cell homing and effector T-cell differentiation (56,57), features that were all enhanced in *Plxna4* KO CTLs. Since we observed that FOXO TFs can regulate the expression of *Plxna4* (35), we speculate that later stages of T-cell activation are characterized by the upregulation of negative regulators of T-cell functions (“immune checkpoint molecules”), which include PD-1 itself but also the PlxnA4 pathway. However, the link between FOXO transcription factors and expression of Plxn4a remain incompletely defined and will need further investigation in future studies.

In terms of clinical management, biomarkers of tumor response to ICIs are needed to help guide treatment strategy. Our results suggest that expression of *PLXNA4* in circulating CTLs could be used as an early, non-invasive biomarker for monitoring patients’ responses to immune checkpoint blockade. In line with our observations, changes in T cell subsets of metastatic melanoma patients were reported to occur within a short period after initiating ICI therapy (58). Although our CTL sampling was done in a prospective manner and larger cohorts of patients will be needed to further confirm our clinical results, the current data well-position PlexinA4 expression in circulating CTLs as a potential biomarker of disease or response to immunotherapy.

### **Acknowledgements**

The authors thank S. Willox, A. Tzoumpa, E. Achten, C. Serrano, J. Grieten, R. Tavares and M. Cogels for their technical assistance. *Plxna4*-KO mice were kindly offered by Dr. Castellani (Institut NeuroMyoGène, Université de Lyon, France). *Sema6a*-mice were kindly offered by Prof. Dr. Pasterkamp (Dept. of Translational Neuroscience, University Medical Center Utrecht, The Netherlands). LCMV-OVA virus was a kind gift from Prof. Dr. Pinschewer (University of Basel, Switzerland). Flow cytometry data was generated with the support from the VIB FACS Expertise Center.

### **Author Contributions**

W.C. and A.I.O. designed the study, performed all experiments, acquired data, performed data analysis, interpreted all data and wrote the manuscript. E.L., Y.V.H., O.B. and J.C.M. provided all the clinical samples and contributed to the scientific discussion. S.R. and H.H.V.A. assisted in experimental work. J.S. and S.T.C. provided technical support. R.M. performed *in vitro* assays. A.K. performed FACS sorting experiments. A.D.G., V.F., L.T. and B.M.C. contributed to the scientific discussion. M.D.M. performed all the cloning and helped with experimental design. M.M. designed the study, conducted scientific direction, interpreted data and helped writing the manuscript.

## **References**

1. Chen DS, Mellman I. Oncology meets immunology: the cancer-immunity cycle. *Immunity* **2013**;39:1-10
2. Kruger S, Ilmer M, Kobold S, Cadilha BL, Endres S, Ormanns S, *et al.* Advances in cancer immunotherapy 2019 - latest trends. *J Exp Clin Cancer Res* **2019**;38:268
3. Galluzzi L, Chan TA, Kroemer G, Wolchok JD, Lopez-Soto A. The hallmarks of successful anticancer immunotherapy. *Sci Transl Med* **2018**;10
4. Fridman WH, Pages F, Sautes-Fridman C, Galon J. The immune contexture in human tumours: impact on clinical outcome. *Nat Rev Cancer* **2012**;12:298-306
5. Teng MW, Ngiow SF, Ribas A, Smyth MJ. Classifying Cancers Based on T-cell Infiltration and PD-L1. *Cancer Res* **2015**;75:2139-45
6. Perala N, Sariola H, Immonen T. More than nervous: the emerging roles of plexins. *Differentiation* **2012**;83:77-91
7. He Z, Wang KC, Koprivica V, Ming G, Song HJ. Knowing how to navigate: mechanisms of semaphorin signaling in the nervous system. *Sci STKE* **2002**;2002:re1
8. Kumanogoh A, Kikutani H. Immunological functions of the neuropilins and plexins as receptors for semaphorins. *Nat Rev Immunol* **2013**;13:802-14
9. Capparuccia L, Tamagnone L. Semaphorin signaling in cancer cells and in cells of the tumor microenvironment--two sides of a coin. *J Cell Sci* **2009**;122:1723-36
10. Suto F, Murakami Y, Nakamura F, Goshima Y, Fujisawa H. Identification and characterization of a novel mouse plexin, plexin-A4. *Mech Dev* **2003**;120:385-96
11. Battistini C, Tamagnone L. Transmembrane semaphorins, forward and reverse signaling: have a look both ways. *Cell Mol Life Sci* **2016**;73:1609-22

12. Fujisawa H. Discovery of semaphorin receptors, neuropilin and plexin, and their functions in neural development. *J Neurobiol* **2004**;59:24-33
13. Suto F, Ito K, Uemura M, Shimizu M, Shinkawa Y, Sanbo M, *et al.* Plexin-a4 mediates axon-repulsive activities of both secreted and transmembrane semaphorins and plays roles in nerve fiber guidance. *J Neurosci* **2005**;25:3628-37
14. Tawarayama H, Yoshida Y, Suto F, Mitchell KJ, Fujisawa H. Roles of semaphorin-6B and plexin-A2 in lamina-restricted projection of hippocampal mossy fibers. *J Neurosci* **2010**;30:7049-60
15. Wen H, Lei Y, Eun SY, Ting JP. Plexin-A4-semaphorin 3A signaling is required for Toll-like receptor- and sepsis-induced cytokine storm. *J Exp Med* **2010**;207:2943-57
16. Kang S, Nakanishi Y, Kioi Y, Okuzaki D, Kimura T, Takamatsu H, *et al.* Semaphorin 6D reverse signaling controls macrophage lipid metabolism and anti-inflammatory polarization. *Nat Immunol* **2018**;19:561-70
17. Casazza A, Laoui D, Wenes M, Rizzolio S, Bassani N, Mambretti M, *et al.* Impeding macrophage entry into hypoxic tumor areas by Sema3A/Nrp1 signaling blockade inhibits angiogenesis and restores antitumor immunity. *Cancer Cell* **2013**;24:695-709
18. Yamamoto M, Suzuki K, Okuno T, Ogata T, Takegahara N, Takamatsu H, *et al.* Plexin-A4 negatively regulates T lymphocyte responses. *Int Immunol* **2008**;20:413-20
19. Flatz L, Hegazy AN, Bergthaler A, Verschoor A, Claus C, Fernandez M, *et al.* Development of replication-defective lymphocytic choriomeningitis virus vectors for the induction of potent CD8+ T cell immunity. *Nat Med* **2010**;16:339-45
20. Eisenhauer EA, Therasse P, Bogaerts J, Schwartz LH, Sargent D, Ford R, *et al.* New response evaluation criteria in solid tumours: revised RECIST guideline (version 1.1). *Eur J Cancer* **2009**;45:228-47
21. Hamm A, Prenen H, Van Delm W, Di Matteo M, Wenes M, Delamarre E, *et al.* Tumour-educated circulating monocytes are powerful candidate biomarkers for diagnosis and disease follow-up of colorectal cancer. *Gut* **2016**;65:990-1000
22. Yaron A, Huang PH, Cheng HJ, Tessier-Lavigne M. Differential requirement for Plexin-A3 and -A4 in mediating responses of sensory and sympathetic neurons to distinct class 3 Semaphorins. *Neuron* **2005**;45:513-23
23. Kigel B, Rabinowicz N, Varshavsky A, Kessler O, Neufeld G. Plexin-A4 promotes tumor progression and tumor angiogenesis by enhancement of VEGF and bFGF signaling. *Blood* **2011**;118:4285-96

24. Podojil JR, Chiang MY, Ifergan I, Copeland R, Liu LN, Maloveste S, *et al.* B7-H4 Modulates Regulatory CD4(+) T Cell Induction and Function via Ligation of a Semaphorin 3a/Plexin A4/Neuropilin-1 Complex. *J Immunol* **2018**;201:897-907
25. Suda T, Liu D. Hydrodynamic gene delivery: its principles and applications. *Mol Ther* **2007**;15:2063-9
26. Girard JP, Moussion C, Forster R. HEVs, lymphatics and homeostatic immune cell trafficking in lymph nodes. *Nat Rev Immunol* **2012**;12:762-73
27. Sackstein R, Schatton T, Barthel SR. T-lymphocyte homing: an underappreciated yet critical hurdle for successful cancer immunotherapy. *Lab Invest* **2017**;97:669-97
28. Kong Y, Janssen BJ, Malinauskas T, Vangoor VR, Coles CH, Kaufmann R, *et al.* Structural Basis for Plexin Activation and Regulation. *Neuron* **2016**;91:548-60
29. Faroudi M, Hons M, Zachacz A, Dumont C, Lyck R, Stein JV, *et al.* Critical roles for Rac GTPases in T-cell migration to and within lymph nodes. *Blood* **2010**;116:5536-47
30. Gomez M, Tybulewicz V, Cantrell DA. Control of pre-T cell proliferation and differentiation by the GTPase Rac-I. *Nat Immunol* **2000**;1:348-52
31. Morris MA, Gibb DR, Picard F, Brinkmann V, Straume M, Ley K. Transient T cell accumulation in lymph nodes and sustained lymphopenia in mice treated with FTY720. *Eur J Immunol* **2005**;35:3570-80
32. Boussiotis VA. Molecular and Biochemical Aspects of the PD-1 Checkpoint Pathway. *N Engl J Med* **2016**;375:1767-78
33. Staron MM, Gray SM, Marshall HD, Parish IA, Chen JH, Perry CJ, *et al.* The transcription factor FoxO1 sustains expression of the inhibitory receptor PD-1 and survival of antiviral CD8(+) T cells during chronic infection. *Immunity* **2014**;41:802-14
34. Delpoux A, Lai CY, Hedrick SM, Doedens AL. FOXO1 opposition of CD8(+) T cell effector programming confers early memory properties and phenotypic diversity. *Proc Natl Acad Sci U S A* **2017**;114:E8865-E74
35. Paap RH, Oosterbroek S, Wagemans C, von Oerthel L, Schellevis RD, Vastenhouwen van der Linden AJA, *et al.* FoxO6 affects Plxn4-mediated neuronal migration during mouse cortical development. *Proc Natl Acad Sci U S A* **2016**;113:E7087-E96
36. Salcher S, Spoden G, Hagenbuchner J, Fuhrer S, Kaserer T, Tollinger M, *et al.* A drug library screen identifies Carbenoxolone as novel FOXO inhibitor that overcomes FOXO3-mediated chemoprotection in high-stage neuroblastoma. *Oncogene* **2020**;39:1080-97
37. Ribas A, Wolchok JD. Cancer immunotherapy using checkpoint blockade. *Science* **2018**;359:1350-5

38. Sharma A, Verhaagen J, Harvey AR. Receptor complexes for each of the Class 3 Semaphorins. *Front Cell Neurosci* **2012**;6:28
39. Greten FR, Grivennikov SI. Inflammation and Cancer: Triggers, Mechanisms, and Consequences. *Immunity* **2019**;51:27-41
40. Pascoe HG, Wang Y, Zhang X. Structural mechanisms of plexin signaling. *Prog Biophys Mol Biol* **2015**;118:161-8
41. Bustelo XR, Sauzeau V, Berenjano IM. GTP-binding proteins of the Rho/Rac family: regulation, effectors and functions in vivo. *Bioessays* **2007**;29:356-70
42. Roney KE, O'Connor BP, Wen H, Holl EK, Guthrie EH, Davis BK, *et al.* Plexin-B2 negatively regulates macrophage motility, Rac, and Cdc42 activation. *PLoS One* **2011**;6:e24795
43. Vikis HG, Li W, Guan KL. The plexin-B1/Rac interaction inhibits PAK activation and enhances Sema4D ligand binding. *Genes Dev* **2002**;16:836-45
44. Zhang N, Bevan MJ. CD8(+) T cells: foot soldiers of the immune system. *Immunity* **2011**;35:161-8
45. Suto F, Tsuboi M, Kamiya H, Mizuno H, Kiyama Y, Komai S, *et al.* Interactions between plexin-A2, plexin-A4, and semaphorin 6A control lamina-restricted projection of hippocampal mossy fibers. *Neuron* **2007**;53:535-47
46. Junqueira Alves C, Yotoko K, Zou H, Friedel RH. Origin and evolution of plexins, semaphorins, and Met receptor tyrosine kinases. *Sci Rep* **2019**;9:1970
47. Haklai-Topper L, Mlechkovich G, Savariego D, Gokhman I, Yaron A. Cis interaction between Semaphorin6A and Plexin-A4 modulates the repulsive response to Sema6A. *EMBO J* **2010**;29:2635-45
48. Rozbesky D, Verhagen MG, Karia D, Nagy GN, Alvarez L, Robinson RA, *et al.* Structural basis of semaphorin-plexin cis interaction. *EMBO J* **2020**;39:e102926
49. Cagnoni G, Tamagnone L. Semaphorin receptors meet receptor tyrosine kinases on the way of tumor progression. *Oncogene* **2014**;33:4795-802
50. Melero I, Rouzaut A, Motz GT, Coukos G. T-cell and NK-cell infiltration into solid tumors: a key limiting factor for efficacious cancer immunotherapy. *Cancer Discov* **2014**;4:522-6
51. Mahoney KM, Rennert PD, Freeman GJ. Combination cancer immunotherapy and new immunomodulatory targets. *Nat Rev Drug Discov* **2015**;14:561-84

52. Tumeh PC, Harview CL, Yearley JH, Shintaku IP, Taylor EJ, Robert L, *et al.* PD-1 blockade induces responses by inhibiting adaptive immune resistance. *Nature* **2014**;515:568-71
53. Brunner-Weinzierl MC, Rudd CE. CTLA-4 and PD-1 Control of T-Cell Motility and Migration: Implications for Tumor Immunotherapy. *Front Immunol* **2018**;9:2737
54. Wei SC, Duffy CR, Allison JP. Fundamental Mechanisms of Immune Checkpoint Blockade Therapy. *Cancer Discov* **2018**;8:1069-86
55. Oestreich KJ, Yoon H, Ahmed R, Boss JM. NFATc1 regulates PD-1 expression upon T cell activation. *J Immunol* **2008**;181:4832-9
56. Luo CT, Li MO. Foxo transcription factors in T cell biology and tumor immunity. *Semin Cancer Biol* **2018**;50:13-20
57. Hedrick SM, Hess Michelini R, Doedens AL, Goldrath AW, Stone EL. FOXO transcription factors throughout T cell biology. *Nat Rev Immunol* **2012**;12:649-61
58. Valpione S, Galvani E, Tweedy J, Mundra PA, Banyard A, Middlehurst P, *et al.* Immune-awakening revealed by peripheral T cell dynamics after one cycle of immunotherapy. *Nat Cancer* **2020**;1:210-21

## **Figure Legends**

### **Figure 1. Genetic knockout of *Plxna4* in the stroma or in the hematopoietic lineage abates tumor progression and increases CTL infiltration.**

(A) Subcutaneous LLC tumor growth and (B) weight in WT and *Plxna4* KO mice. (C) Flow cytometric analysis of CTLs in the tumor-draining lymph node (TdLN) from WT and *Plxna4* KO mice bearing subcutaneous LLC tumors. (D) Histological quantification of CTLs in the inner tumor bed, (E) representative micrographs (scale, 50  $\mu$ m) and (F) paired analysis of the inner (core) and outer (border) tumor areas of LLC tumor sections obtained from WT and *Plxna4* KO tumor-bearing mice. (G) Flow cytometric analysis of CTLs in the TdLN and (H) orthotopic B16F10 tumors from WT and *Plxna4* KO tumor-bearing mice. (I) LLC tumor growth and (J) tumor weight of lethally irradiated WT mice reconstituted with WT (WT $\rightarrow$ WT) or *Plxna4* KO (KO $\rightarrow$ WT) bone marrow cells. (K) Tumor growth and (L) tumor weight in an orthotopic E0771 breast cancer model. (M) Flow cytometric analysis of CTLs in the TdLN and (N) primary tumor from WT $\rightarrow$ WT and *Plxna4* KO $\rightarrow$ WT chimeras. For the *in vivo* experiments, n= 4-8 mice per group. \*p < 0.05, \*\*p < 0.01, \*\*\*p < 0.001 and \*\*\*\*p < 0.0001 versus WT (A-D, G and H), CTLs in the tumor border (F) and versus WT $\rightarrow$ WT (I-N). All graphs show mean  $\pm$  SEM.

### **Figure 2. *Plxna4* expression is dynamically regulated in CTLs.**

(A) Time-course of *Plxna4* expression in purified mouse CD8<sup>+</sup> and CD4<sup>+</sup> T cells activated with anti-CD3/CD28 for 3 days and further expanded in the presence of IL-2. (B) Representative images of PlexinA4 cytospin staining on WT and *Plxna4* KO CTLs before and after 3 days of anti-CD3/CD28 activation (scale, 50  $\mu$ m). (C) Time-course of *PLXNA4* expression in purified human CD8<sup>+</sup> and CD4<sup>+</sup> T cells activated with anti-CD3/CD28 for 3 days and further expanded in the presence of IL-2. (D) *Plxna4* expression in circulating CTLs sorted from healthy mice and orthotopic B16F10 or subcutaneous LLC tumor-bearing mice. (E) *Plxna4* expression in naïve T cells (CD8<sup>+</sup>CD44<sup>Lo</sup>CD62L<sup>Hi</sup>), effector/memory T cells (CD8<sup>+</sup>CD44<sup>Hi</sup>CD62L<sup>Lo</sup>) and central memory T cells (CD8<sup>+</sup>CD44<sup>Hi</sup>CD62L<sup>Hi</sup>) sorted from the circulation and LNs of healthy mice. (F) *Plxna4* expression in naïve T cells (CD8<sup>+</sup>CD44<sup>Lo</sup>CD62L<sup>Hi</sup>), effector/memory T cells (CD8<sup>+</sup>CD44<sup>Hi</sup>CD62L<sup>Lo</sup>), central memory T cells (CD8<sup>+</sup>CD44<sup>Hi</sup>CD62L<sup>Hi</sup>) and terminally exhausted T cells (CD8<sup>+</sup>PD-1<sup>Hi</sup>TIM-3<sup>Hi</sup>) sorted from the circulation, TdLN and B16F10 orthotopic tumors of tumor-bearing mice. (G) *Plxna4* expression in CD8<sup>+</sup>CD4<sup>Lo</sup> and CD8<sup>+</sup>CD4<sup>Hi</sup> T cells sorted from the circulation and liver of hydrodynamically vaccinated mice. For the *in vivo* experiments, n= 3-5 mice per group (D-G). *In vitro* results (A, C) were performed in triplicates and are representative of two independent experiments. \*p < 0.05, \*\*p < 0.01 and \*\*\*p < 0.001 versus naïve and activated mouse CD4<sup>+</sup> T cells (A), naïve and activated CD4<sup>+</sup> human T cells (C), circulating CTLs in healthy mice (D), effector/memory T cells in LNs or corresponding circulating T cell subset (E), effector/memory T cells present in the same tissue or corresponding circulating T cell subset (F), circulating CD8<sup>+</sup>CD44<sup>Hi</sup> T cells and CD8<sup>+</sup>CD44<sup>Hi</sup> T cells in the liver (G). All graphs show mean  $\pm$  SEM.).

**Figure 3. Genetic knockout of *Plxna4* in CTLs increases motility and proliferation via enhanced Rac1 activity.**

(A) *In vitro* proliferation of WT and *Plxna4* KO CTLs upon anti-CD3/CD28 activation showing absolute cell numbers and (B) a representative histogram of Violet Cell Tracer fluorescence intensity, gated on CD8<sup>+</sup> T cells, after 4 days in culture. (C) Transmigration assay of naïve WT and *Plxna4* KO CTLs towards CCL21 and CCL19 chemokines. (D) Transmigration assay of activated WT and *Plxna4* KO CTLs towards CXCL9 and CXCL10 chemokines. (E) Transmigration assay of naïve WT and *Plxna4* KO CTLs towards the CCL21 chemokine, treated with IgG or anti-CCR7. (F) Transmigration assay of activated WT and *Plxna4* KO CTLs towards the CXCL10 chemokine, treated with IgG or anti-CXCR3. (G) GTP-bound Rac1 pull-down assay on activated WT and *Plxna4* KO CTLs. Quantification by densitometry, paired analysis on each individual experiment (left) and a representative image of the western blot (right). (H) Transmigration assay of activated WT and *Plxna4* KO CTLs towards the CXCL10 chemokine, treated with either vehicle or the Rac1 inhibitor NSC23766. (I) *In vitro* proliferation of activated WT and *Plxna4* KO CTLs, treated at day 3 with either vehicle or the Rac1 inhibitor NSC23766. *In vitro* results were performed in triplicates (A, D-F, H and I) or duplicates (C) and are representative of at least two independent experiments. Pull-down assay (G) is represented as the pooled data from four independent experiments (left panel) and the western blot is representative of at least three independent experiments (right panel). \**p* < 0.05, \*\**p* < 0.01, \*\*\**p* < 0.001 and \*\*\*\**p* < 0.0001 versus WT CTLs (A, C and D), IgG-treated WT and *Plxna4* KO CTLs (E and F) and vehicle-treated WT and *Plxna4* KO CTLs (H and I). All graphs show mean ± SEM.

**Figure 4. *Plxna4* KO CTLs show increased homing and proliferation capacity in inflammatory sites.**

(A) Homing of naïve WT and *Plxna4* KO CTLs to the LNs of healthy mice quantified by histology and (B) representative micrograph (scale, 100 µm). (C) Homing of naïve WT and *Plxna4* KO CTLs to the LNs of healthy mice treated with either vehicle or the S1PR inhibitor FTY720. (D) Ratio of CD8<sup>+</sup>CD44<sup>Hi</sup> to CD8<sup>+</sup>CD44<sup>Lo</sup> circulating WT and *Plxna4* KO OT-I T cells in mice 32 hours and 48 hours after LCMV-OVA infection, analyzed by flow cytometry. (E) Tumor homing of activated WT and *Plxna4* KO OT-I T cells to B16F10-OVA tumor-bearing mice assessed by flow cytometry 24 hours and 48 hours after tail vein injection. (F) Flow cytometric analysis of labelled T cells in B16F10-OVA tumors 24 hours after intratumoral injection of activated WT and *Plxna4* KO OT-I T cells. (G) Liver homing of activated WT and *Plxna4* KO OT-I T cells to mice hydrodynamically injected with empty vector (EV) or ovalbumin vector (OVA). (H) Tumor homing of activated WT and *Plxna4* KO OT-I T cells to tumor-bearing mice, injected with B16F10-OVA cancer cells transduced with EV or overexpressing (OE) *Sema3a*, *Sema6a* or *Sema6b*. T cell infiltration was assessed by flow cytometry 24 hours after tail vein injection. (I) Tumor homing of activated WT and *Plxna4* KO OT-I T cells to WT and *Sema6a* KO tumor-bearing mice, injected with B16F10-OVA cancer cells. T-cell infiltration was assessed by flow cytometry 24 hours after tail vein injection. For the *in vivo* experiments, n= 4-5 mice per group. \**p* < 0.05, \*\**p* < 0.01, \*\*\**p* < 0.001 and \*\*\*\**p* < 0.0001 versus WT CTLs (A and C) and WT OT-I T cells (E-I). All graphs show mean ± SEM.

**Figure 5. Adoptive transfer of *Plxna4* KO CTLs leads to improved anti-tumor immunity.**

(A) Tumor growth, (B) tumor weight and (C) representative images of end-stage tumors following adoptive transfer (ACT) of activated WT and *Plxna4* KO OT-I T cells in B16F10-OVA tumor-bearing WT mice (scale, 2 cm). (D) Flow cytometric analysis of intratumoral OT-I<sup>+</sup> T cells in B16F10-OVA tumors isolated 4 days after ACT. (E) Kaplan-Meier overall survival curves. For the *in vivo* experiments, n= 6-8 mice per group. \*p < 0.05 and \*\*\*p < 0.001 versus WT OT-I T cells. All graphs show mean ± SEM.

**Figure 6. *PLXNA4* expression is upregulated in circulating CTLs of metastatic melanoma patients.**

(A) *PLXNA4* expression in isolated CTLs from the circulation of treatment-naïve melanoma patients versus healthy controls. (B) Naïve versus paired immune checkpoint inhibitor (anti-PD-1 alone or in combination with anti-CTLA-4; ICIs) treated melanoma patients 3 weeks after one cycle of treatment. (C) *PLXNA4* expression in isolated CTLs from the circulation of treatment-naïve and paired ICI-treated melanoma patients that clinically responded to ICIs and (D) melanoma patients that did not respond to ICIs. (E) *Plxna4* expression in circulating CTLs isolated from orthotopic B16F10 tumor-bearing mice treated with IgG or anti-PD-1. (F) *PLXNA4* expression in *ex vivo* activated human CD8<sup>+</sup> and CD4<sup>+</sup> WT T cells treated with IgG or anti-PD-1. (G) Weight of end-stage B16F10-OVA tumors receiving ACT of activated WT and *Plxna4* KO OT-I T cells in combination with IgG or anti-PD-1 therapy. (H) Fold change of *Plxna4* expression in *ex vivo* activated mouse CTLs treated with vehicle, anti-PD-1 or Carbenoxolone (CBX). (I) Schematic overview of the data presented. For the patient data (A-D), n= 16 healthy controls, n= 31 treatment naïve melanoma patients and n= 20 ICI-treated melanoma patients (see Table S3). *In vitro* results (F and H) were performed in at least triplicates and are represented as the pooled data from two independent experiments. For the *in vivo* experiment (E and G), n= 5-9 mice per group. \*p < 0.05, \*\*p < 0.01, \*\*\*p < 0.001 and \*\*\*\*p < 0.0001 versus circulating CTLs in healthy individuals (A), circulating CTLs in treatment naïve melanoma patients (B and C), circulating CTLs isolated from IgG-treated mice (E), IgG-treated human CTLs (F), B16F10-OVA tumors receiving ACT of activated WT OT-I T cells and IgG-treated B16F10-OVA tumors (G) and vehicle-treated mouse CTLs (H). All graphs show mean ± SEM.

**Figure 1**

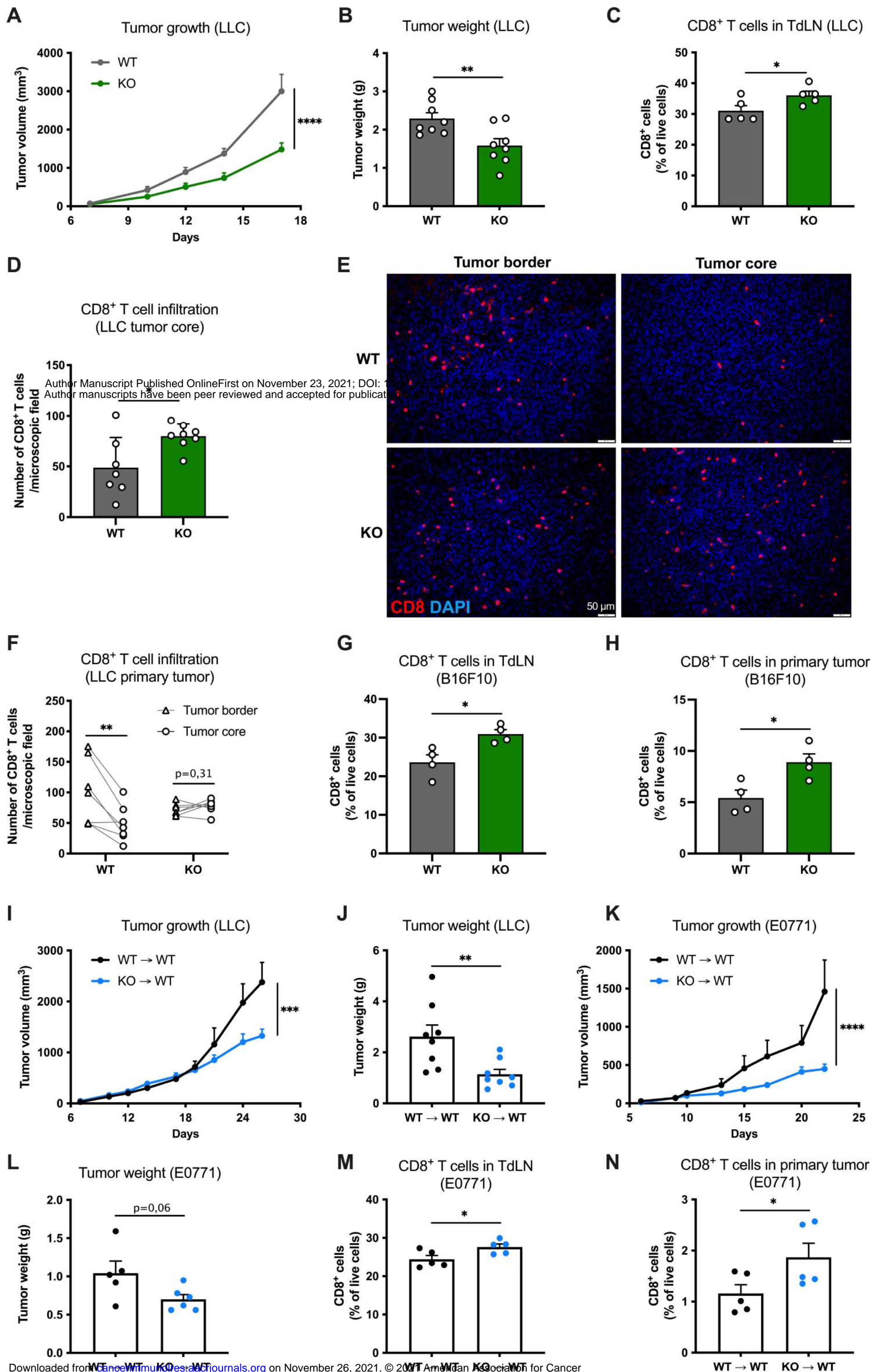


**Figure 2**

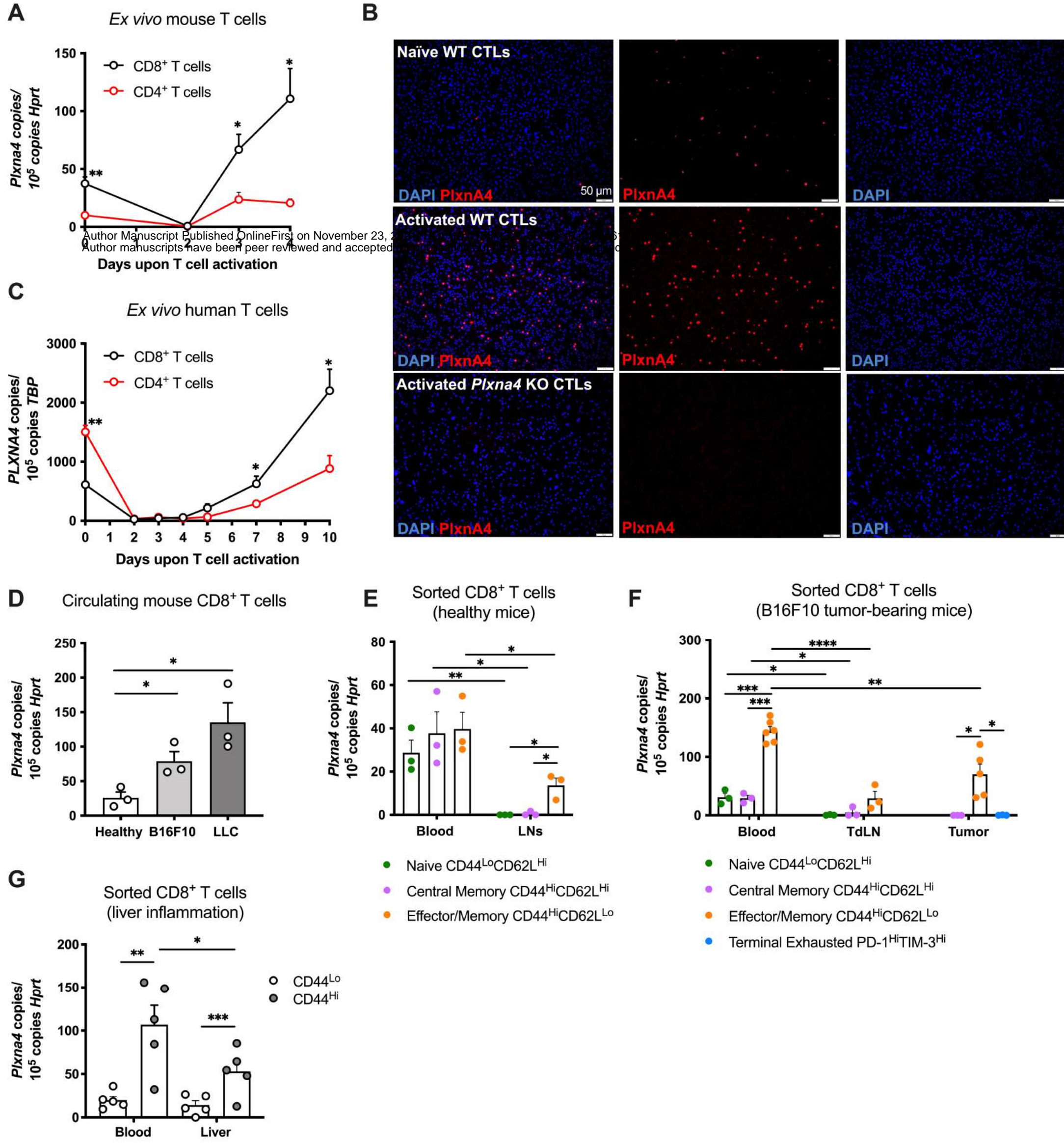


**Figure 3**

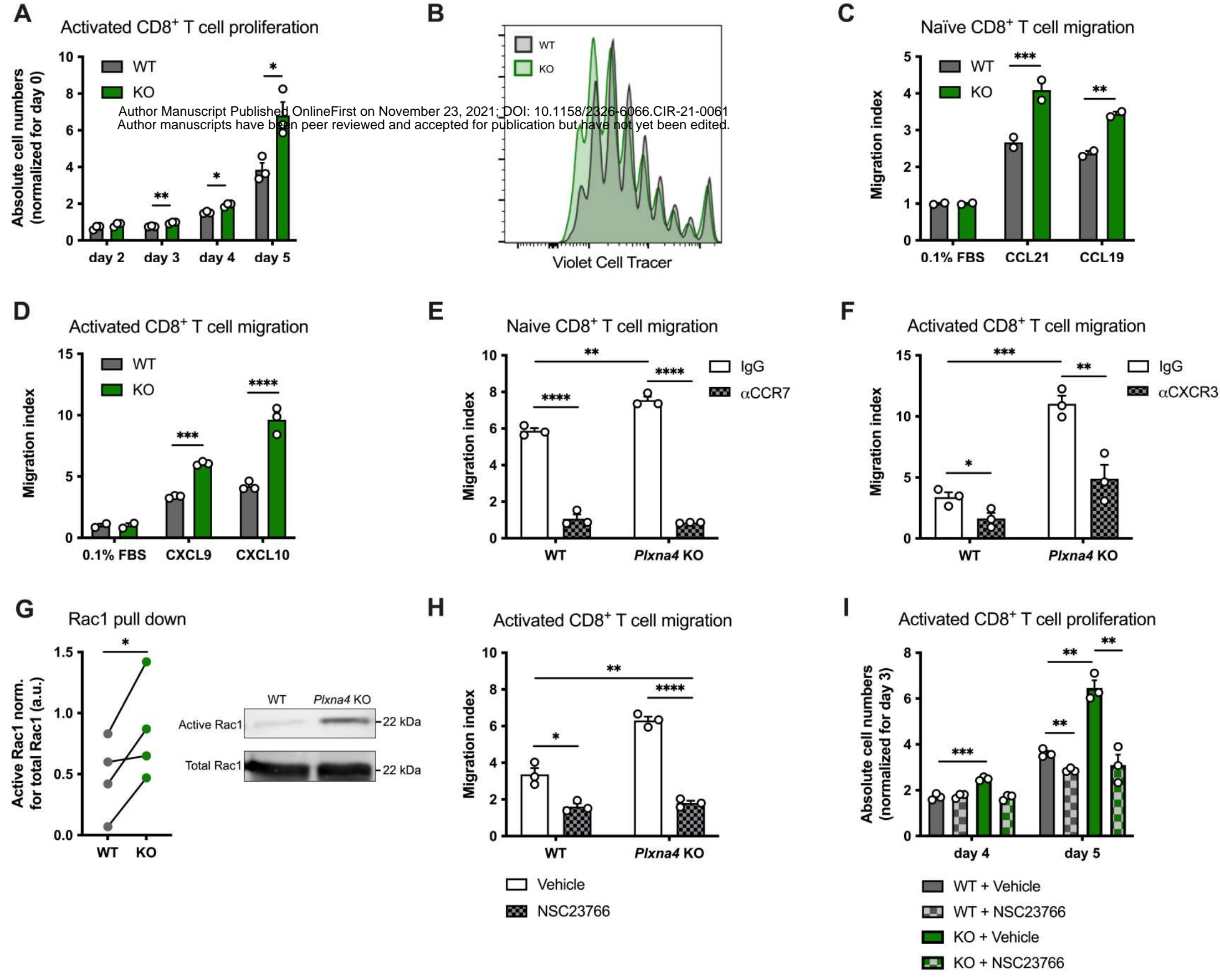


**Figure 4**

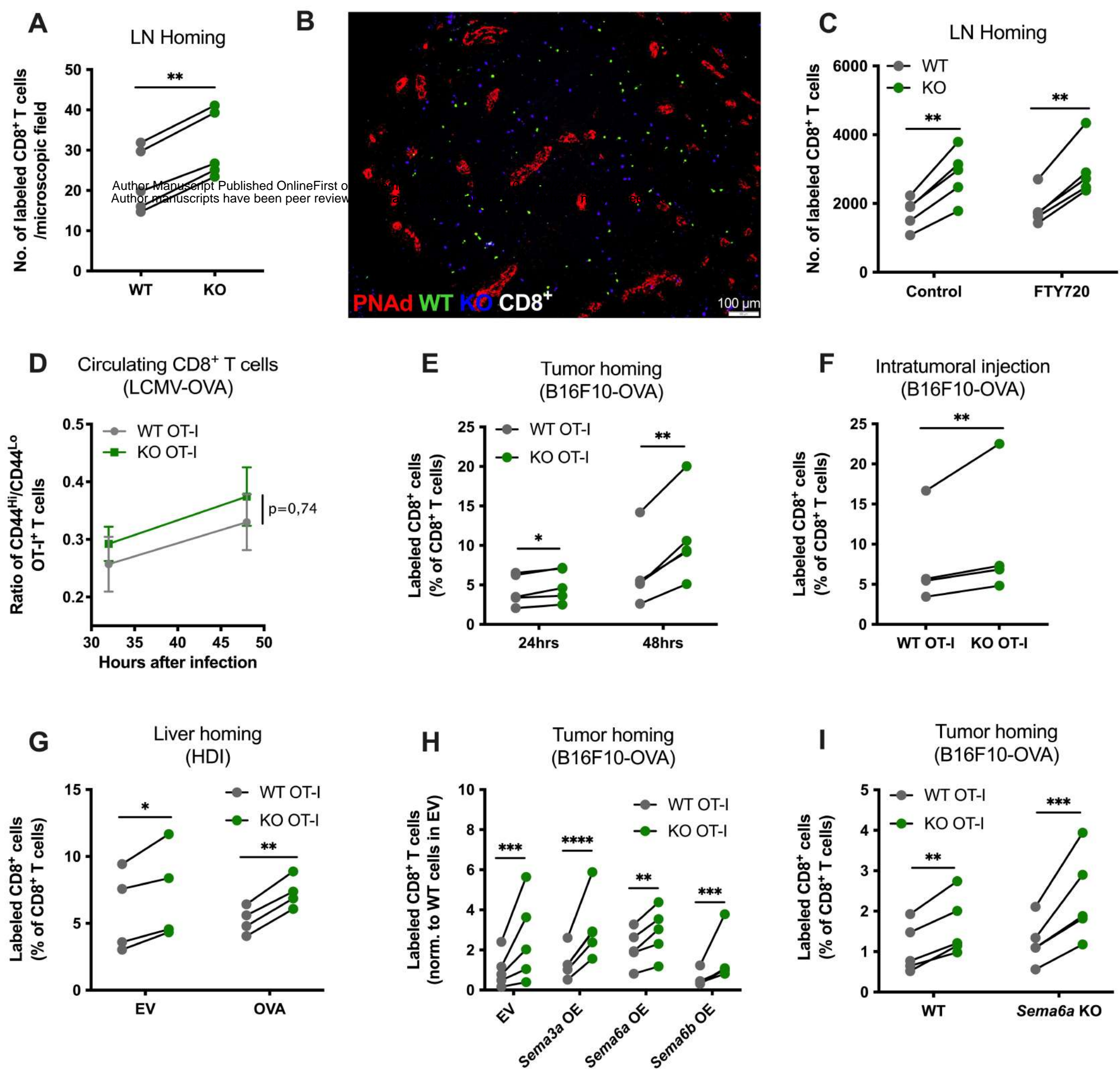
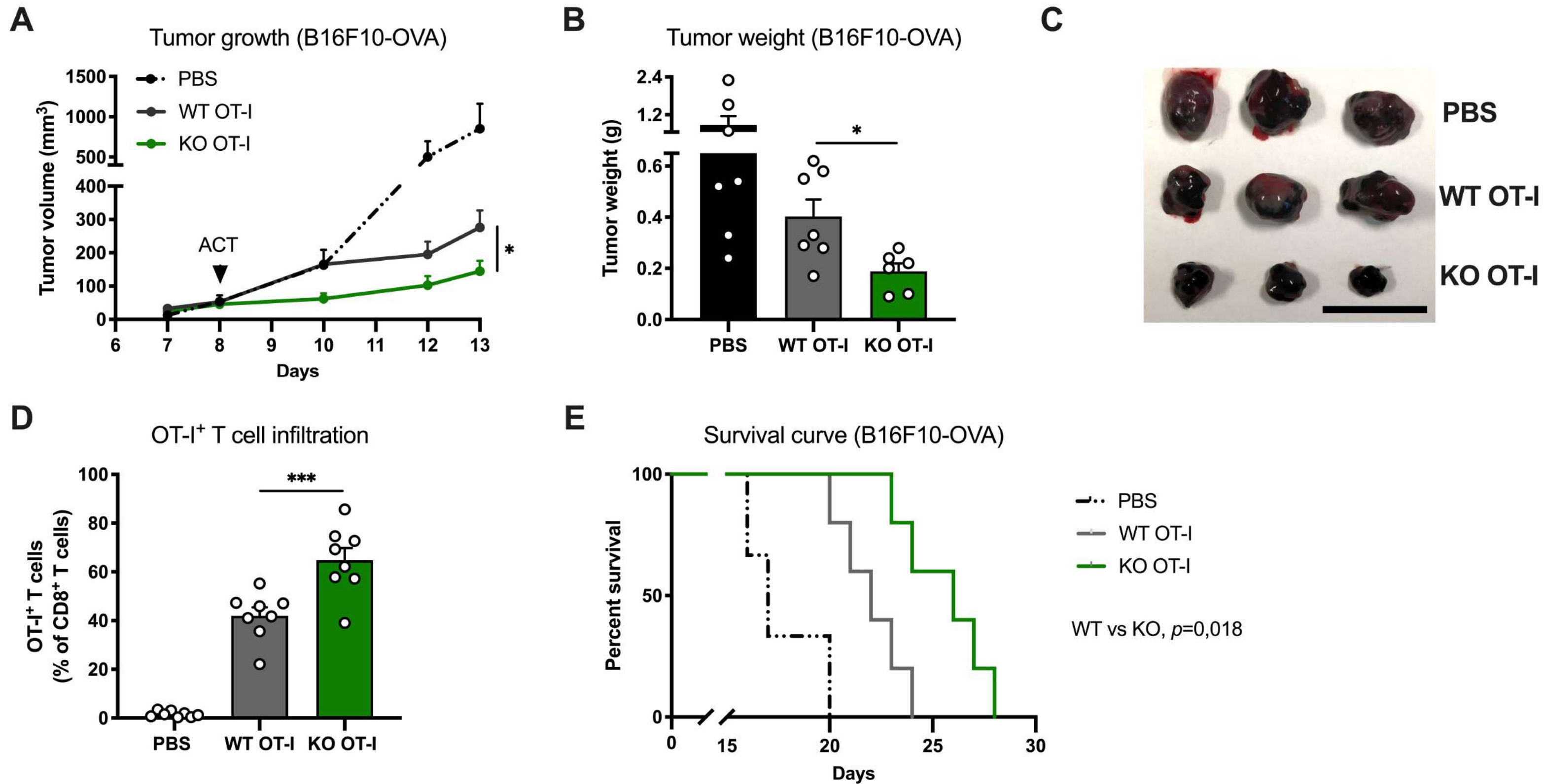


## Figure 5





# Cancer Immunology Research

## PlexinA4 mediates cytotoxic T cell trafficking and exclusion in cancer

Ward Celus, Ana I. Oliveira, Silvia Ravis, et al.

*Cancer Immunol Res* Published OnlineFirst November 23, 2021.

<b>Updated version</b>	Access the most recent version of this article at: doi: <a href="https://doi.org/10.1158/2326-6066.CIR-21-0061">10.1158/2326-6066.CIR-21-0061</a>
<b>Supplementary Material</b>	Access the most recent supplemental material at: <a href="http://cancerimmunolres.aacrjournals.org/content/suppl/2021/11/18/2326-6066.CIR-21-0061.DC1">http://cancerimmunolres.aacrjournals.org/content/suppl/2021/11/18/2326-6066.CIR-21-0061.DC1</a>
<b>Author Manuscript</b>	Author manuscripts have been peer reviewed and accepted for publication but have not yet been edited.

<b>E-mail alerts</b>	<a href="#">Sign up to receive free email-alerts</a> related to this article or journal.
<b>Reprints and Subscriptions</b>	To order reprints of this article or to subscribe to the journal, contact the AACR Publications Department at <a href="mailto:pubs@aacr.org">pubs@aacr.org</a> .
<b>Permissions</b>	To request permission to re-use all or part of this article, use this link <a href="http://cancerimmunolres.aacrjournals.org/content/early/2021/11/18/2326-6066.CIR-21-0061">http://cancerimmunolres.aacrjournals.org/content/early/2021/11/18/2326-6066.CIR-21-0061</a> . Click on "Request Permissions" which will take you to the Copyright Clearance Center's (CCC) Rightslink site.